College of ENGINEERING
VILLANOVA UNIVERSITY

Center for Advanced Communications

Villanova University

ANNUAL REPORT

(10/1/2004 – 9/30/2005)

CLASSIFICATION AND DISCRIMINATION OF SOURCES WITH TIME-VARYING FREQUENCY AND SPATIAL SPECTRA

Submitted to

Office of Naval Research

Grant No. N00014-98-1-0176

Principal Investigators

Moeness G. Amin

Contributors

Prof. Moeness Amin
Prof. Yimin Zhang
Mr. Baha Obeidat
Mr. Pawan Setlur

October 2005

Table of Contents

Executive Summary

Classification and Discrimination of Sources with Time-Varying Frequency and Spatial Spectra

ONR Grant No. N00014-98-1-0176

Moeness Amin (PI)

This report presents the results of the research performed under ONR grant number N00014-98-1-0176 over the period of October 1st, 2004 to September 30th, 2005. The research team working on this project consists of Prof. Moeness Amin (PI), Prof. Yimin Zhang (Research Professor), Mr. Baha Obeidat and Mr. Pawan Setlur (Graduate Students). We have also collaborated with Dr. Thayananthan Thayaparan (Defense Research and Development, Canada), Prof. Ahmad Hoorfar (Villanova University), and Prof. Kehu Yang (Xidian University, China).

The research objective in FY05 evolved around the moving target tracking using time-frequency signal representations. In addition to achieving this objective, the research has progressed on three other fronts, namely, *Sensor configuration in polarized antenna arrays*, *DOA and polarization estimation for wideband sources*, and *Micro-Doppler experiments*. One book chapter, two journal articles, and seven conference papers have been generated from our research efforts in FY05. Below is the summary of the research accomplishments in each of the individual areas. Copies of the principle publications are included in the report.

1. Spatial Polarimetric Time-Frequency Distributions for Moving Target Tracking

We have introduced the spatial polarimetric time-frequency distributions (SPTFDs) as a platform for processing polarized nonstationary signals incident on multiple dual-polarized double-feed antennas. Based on this platform, we have developed the polarimetric time-frequency MUSIC (PTF-MUSIC) methods for direction-of-arrival (DOA) estimation of nonstationary sources with distinct polarization characteristics, and have examined the feasibility of the PTF-MUSIC methods for tracking moving sources with time-varying polarization characteristics. We have demonstrated the significance of polarization diversity in challenging direction finding problems, where the sources are closely spaced, and discuss important issues relevant to utilization of polarization diversity. The SPTFD has the capability of incorporating both the instantaneous polarization information and time-frequency signatures of the different sources in the field of view. The incorporation of specific time-frequency points or regions, where one or more signals reside, enhances signal-to-noise ratio (SNR) and allows source discrimination and source elimination. This, in turn, leads to DOA performance improvement and reductions in the required number of array sensors. The PTF-MUSIC significantly outperforms the existing time-frequency MUSIC, polarimetric MUSIC and conventional MUSIC direction finding techniques.

2. DOA and Polarization Estimation for Wideband Sources

We have presented an approach to direction-of-arrival (DOA) and polarization estimations of far-field wideband signals using an array of cross-polarized dual-feed sensors. The wideband signals are decomposed into a set of narrowband signals. Coherent signal subspace processing is then applied to dimension-extended source signal correlation matrices at different narrowband frequencies, leading to the construction of single signal subspace. The utilization of polarization diversity through the use of a dual-feed cross-polarized array to process the polarized signal arrivals lends an additional degree of freedom, leading to performance improvement over the case where a single-polarization array is used.

3. Sensor Configurations in Nonstationary Array Processing

We have developed the spatio-polarimetric correlation as a framework to evaluate the direction-of-arrival estimation performance of different receiver configurations employing double-feed dual-polarized array as well as arrays of single-feed single-polarized elements. Single- and dual-polarized array configurations are often used in imaging and radar applications. The spatio-polarimetric correlation coefficients are derived for several array reconfigurations and used to provide a configuration-based performance comparison based on spatial resolution and grating lobes.

4. Micro-Doppler Experiments

We have conducted several important indoor experiments for detecting micro-Doppler signatures of some commonly encountered indoor targets. Targets in real life have vibrating and rotating parts in addition to the translations endured by the target. The target itself might either be rotating or vibrating with no translation, a motion is described mechanically as simple-harmonic motion (SHM). Such nonlinear motions then induce additional frequency modulations around the Doppler, this is termed micro-Doppler effect. Micro-Doppler has many applications for target recognition and classification. Experiments were designed to image targets which induce micro-Doppler like signatures. The targets were primarily a rotating fan and a toy train moving on a circular track. The experiments were conducted using CW (Continuous Wave) radars. These radars measure only the real component of target returns. Time-frequency techniques were used to depict the instantaneous frequency of the target. The objective of the experiments was to compute the frequency of vibrations or rotations. In this report, we introduce the problem statement, and propose a model for Micro-Doppler. Experimental setup is described, and simulation and experimental results are also presented.

List of Publications

Journal Papers

[1] Y. Zhang, B. Obeidat, and M. G. Amin, "Spatial polarimetric time-frequency distributions for direction-of-arrival estimations," IEEE Transactions on Signal Processing (in press).

[2] Y. Zhang, K. Yang, and M. G. Amin, "Subband array implementations for space-time adaptive processing," EURASIP Journal on Applied Signal Processing, vol. 2005, no. 1, pp. 99-111, Jan. 2005.

Book Chapter

[3]* Y. Zhang, B. Obeidat, and M. G. Amin, "Polorimetric time-frequency MUSIC for direction finding of moving sources with time-varying polarizations," in S.Chandran (ed.), Advances in Direction of Arrival Estimation, Boston, MA: Artech House (in press).

Conference papers

[4] Y. Zhang, B. Obeidat, and M. G. Amin, "Nonstationary array processing for sources with time-varying polarizations," Annual Asilomar Conference on Signals, Systems, and Computers, Pacific Grove, CA, Nov. 2004.

[5]* B. Obeidat, Y. Zhang, and M. G. Amin, "DOA and polarization estimation for wideband sources," Annual Asilomar Conference on Signals, Systems, and Computers, Pacific Grove, CA, Nov. 2004.

[6] B. A. Obeidat, Y. Zhang, and M. G. Amin, "Nonstationary array processing for tracking moving targets with time-varying polarizations," IEEE International Conference on Acoustics, Speech, and Signal Processing, Philadelphia, PA, March 2005.

[7]* B. Obeidat, M. G. Amin, Y. Zhang, A. Hoorfar, "Sensor configuration in polarized antenna arrays," IEEE International Symposium on Signal Processing and its Applications, Sydney, Australia, Aug. 2005.

[8] P. Setlur, M. Amin, and T. Thayaparan, "Micro-Doppler signal estimation for vibrating and rotating targets," IEEE Internal Symposium on Signal Processing and its Applications, Sydney, Australia, August 2005.

[9] B. A. Obeidat, Y. Zhang, and M. G. Amin, "Performance analysis of DOA estimation using dual-polarized antenna arrays," IEEE International Symposium on Signal Processing and Information Technology, Athens, Greece, Dec. 2005.

[10] P. Setlur, M. Amin, F. Ahmad, and T. Thayaparan, "Indoor imaging of targets enduring simple harmonic motion using Doppler radars," IEEE International Symposium on Signal processing and Information Technology, Athens, Greece, Dec. 2005.

Publications with * are included in "Selected Publications."

Selected Publications

1. Polorimetric time-frequency MUSIC for direction finding of moving sources with time-varying polarizations

2. DOA and polarization estimation for wideband sources

3. Sensor configuration in polarized antenna arrays

4. Micro-Doppler experiments

Polarimetric Time-Frequency MUSIC for Direction Finding of Moving Sources with Time-Varying Polarizations

Yimin Zhang, Baha A. Obeidat, Moeness G. Amin

Abstract: The spatial polarimetric time-frequency distributions (SPTFDs) have been introduced as a platform for processing polarized nonstationary signals incident on multiple dual-polarized double-feed antennas. Based on this platform, the polarimetric time-frequency MUSIC (PTF-MUSIC) methods have been developed for direction-of-arrival (DOA) estimation of nonstationary sources with distinct polarization characteristics. In this paper, we examine the feasibility of the PTF-MUSIC methods for tracking of moving sources with time-varying polarization characteristics. We demonstrate the significance of polarization diversity in challenging direction finding problems, where the sources are closely spaced, and discuss important issues relevant to utilization of polarization diversity. The SPTFD has the capability of incorporating both the instantaneous polarization information and time-frequency signatures of the different sources in the field of view. The incorporation of specific time-frequency points or regions, where one or more signals reside, enhances signal-to-noise ratio (SNR) and allows source discrimination and source elimination. This, in turn, leads to DOA performance improvement and reductions in the required number of array sensors. The PTF-MUSIC significantly outperforms the existing time-frequency MUSIC, polarimetric MUSIC and conventional MUSIC direction finding techniques.

1. Introduction

Time-frequency distributions (TFDs) have been used for nonstationary signal analysis and synthesis in various areas, including speech, biomedicine, automotive industry, and machine monitoring [1, 2, 3]. Over the past few years, the spatial dimension has been incorporated, along with the time and frequency variables, into quadratic and higher-order TFDs, and led to the introduction of spatial time-frequency distributions (STFDs) as a powerful tool for nonstationary array signal processing [4, 5, 6]. The relationship between the TFDs of the sensor data to the TFDs of the individual source waveforms is defined by the steering, or the mixing, matrix, and was found to be similar to that encountered in the traditional data covariance matrix approach to array processing. This similarity has allowed subspace-based estimation methods to be applied to time-frequency signal representations, utilizing the source instantaneous frequency for direction finding. It has been shown that the MUSIC [7, 8], maximum likelihood [9], and ESPRIT [10] techniques based on SPTFDs outperform their counterparts that are based on covariance matrices, when the sources are of nonstationary temporal characteristics.

Polarization and polarization diversities, on the other hand, are commonly used in wireless communications and various types of radar systems [11, 12]. Antenna and target polarization properties are widely employed in remote sensing and synthetic aperture radar (SAR) applications [13, 14, 15]. Airborne and spaceborne platforms as well as meteorological radars include polarization information [16, 17]. Additionally, polarization plays an effective role in identification of targets in the presence of clutter [18, 19], and has also been incorporated in antenna arrays to improve signal parameter estimations, including DOA and time-of-arrival (TOA) [20, 21].

To combine time-frequency (t-f) signal representations and polarimetric signal processing, we have introduced the spatial polarimetric time-frequency distributions (SPTFDs) for double-feed dual-polarized arrays, which allow the utilization of both the t-f and polarization signatures of the sources in the field of view [22, 23]. We then used the SPTFD to develop the polarimetric time-frequency MUSIC (PTF-MUSIC) technique, which is formulated based on the source t-f and polarization properties. This new technique is employed for DOA estimation of polarized nonstationary signals and shown to outperform the MUSIC techniques that only incorporate either the t-f or the polarimetric source characteristics [23]. The application of the SPTFDs to an ESPRIT-like method was introduced in [22,24].

In this paper, we examine the feasibility of the PTF-MUSIC methods for tracking of moving sources with time-varying polarization characteristics. We demonstrate the significance of polarization diversity in direction finding problems in which the sources are closely spaced, and discuss the necessary treatment of the data samples to effectively utilize the polarization diversity. The SPTFD incorporates the instantaneous polarization information at selected auto-term t-f points where the energy of desired source signals is localized. The selection of t-f regions in constructing the SPTFD matrices not only reduces noise, but also enables source exclusion from post-eigendecomposition and subspace estimation. Reduction of the number of sources reduces the required number of array sensors and lead to performance enhancement. As a result, PTF-MUSIC outperforms existing polarimetric MUSIC technique.

This paper is organized as follows. Section 0 discusses the signal model and briefly reviews TFDs and STFDs. Section 0 considers dual-polarized antenna arrays and introduces

the concept of spatial polarimetric time-frequency distributions (SPTFDs). The PTF-MUSIC algorithm is proposed in Section 0. Section 0 considers the spatio-polarimetric correlation which is a useful parameter to measure the closeness between two sources in the joint spatial and polarimetric domains. Section 0 considers DOA tracking of moving sources with time-varying polarization characteristics. Computer simulations, demonstrating the effectiveness of the proposed methods, are provided in Section 0.

Throughout this paper, vectors and matrices are denoted by lower-case bold and upper-case letters, respectively. The operation $E[\cdot]$ denotes expectation, $(\cdot)^*$ denotes complex conjugate, $(\cdot)^T$ denotes transpose, and $(\cdot)^H$ denotes conjugate transpose (Hermitian). We use $(\cdot)^{[i]}$ to denote polarization, $\|\cdot\|$ vector norm, $\otimes$ denotes the Kronecker product operator, and $\circ$ denotes the Hadamard product operator.

2. Signal Model

2.1 Time-Frequency Distributions (TFDs)

The Cohen's class of TFDs of a signal $x(t)$ is defined as [1]

$$D_{xx}(t,f) = \iint \phi(t-u,\tau)x(u+\frac{\tau}{2})x^*(u-\frac{\tau}{2})e^{-j2\pi f\tau}dud\tau\,, \qquad (1)$$

where t and f represent the time and frequency indexes, respectively, $\phi(t,\tau)$ is the t-f kernel, and τ is the time-lag variable. In this paper, all the integrals are from $-\infty$ to ∞.

The cross-term TFD of two signals $x_i(t)$ and $x_k(t)$ is defined by

$$D_{x_ix_k}(t,f) = \iint \phi(t-u,\tau)x_i(u+\frac{\tau}{2})x_k^*(u-\frac{\tau}{2})e^{-j2\pi f\tau}dud\tau\,. \qquad (2)$$

2.2 Spatial Time-Frequency Distributions (STFDs)

The STFDs have been developed for single-polarized antenna arrays [4, 5, 6]. Consider n narrowband signals impinging on an array of m single-polarized antenna elements. The following linear data model is assumed,

$$\mathbf{x}(t) = \mathbf{y}(t) + \mathbf{n}(t) = \mathbf{A}(\mathbf{\Phi})\mathbf{s}(t) + \mathbf{n}(t), \qquad (3)$$

where the $m \times n$ matrix $\mathbf{A}(\mathbf{\Phi}) = [\mathbf{a}(\phi_1), \mathbf{a}(\phi_2), \ldots, \mathbf{a}(\phi_n)]$ is the mixing matrix that holds the spatial information of the n signals, $\mathbf{\Phi} = [\phi_1, \phi_2, \ldots, \phi_n]$ and $\mathbf{a}(\phi_i)$ is the spatial signature for source i. Each element of the $n \times 1$ vector $\mathbf{s}(t) = [s_1(t), s_2(t), \ldots, s_n(t)]^T$ is a mono-component signal. Due to the signal mixing occurring at each sensor, the elements of the $m \times 1$ sensor data vector $\mathbf{x}(t)$ are multi-component signals. $\mathbf{n}(t)$ is an $m \times 1$ additive noise vector that consists of independent zero-mean, white and Gaussian distributed processes.

The STFD of a data vector $\mathbf{x}(t)$ is expressed as [4]

$$\mathbf{D}_{\mathbf{xx}}(t,f) = \iint \phi(t-u,\tau)\mathbf{x}(u+\frac{\tau}{2})\mathbf{x}^H(u-\frac{\tau}{2})e^{-j2\pi f\tau}\,du\,d\tau\,, \qquad (4)$$

where the (i,k) th element of $\mathbf{D}_{\mathbf{xx}}(t,f)$ is given by Eq. (2) for $i,k = 1,2,\ldots,m$. The noise-free STFD is obtained by substituting Eq. (3) in Eq. (4), resulting in

$$\mathbf{D}_{\mathbf{xx}}(t,f) = \mathbf{A}(\mathbf{\Phi})\mathbf{D}_{\mathbf{ss}}(t,f)\mathbf{A}^H(\mathbf{\Phi})\,, \qquad (5)$$

where $\mathbf{D}_{\mathbf{ss}}(t,f)$ is the TFD matrix of $\mathbf{s}(t)$ which consists of auto- and cross-source TFDs. With the presence of the noise, which is uncorrelated with the signals, the expected value of $\mathbf{D}_{\mathbf{xx}}(t,f)$ yields

$$E[\mathbf{D}_{xx}(t,f)] = \mathbf{A}(\mathbf{\Phi})E[\mathbf{D}_{ss}(t,f)]\mathbf{A}^H(\mathbf{\Phi}) + \sigma^2\mathbf{I}, \quad (6)$$

where σ^2 is the noise power and $\mathbf{I}$ is the identity matrix.

Equation (6) relates the STFD matrix to the source TFD matrix. It is similar to the formula that is commonly used in narrowband array processing problems, relating the source covariance matrix to the sensor spatial covariance matrix. It is clear, therefore, that the two subspaces spanned by the principle eigenvectors of $\mathbf{D}_{xx}(t,f)$ and the columns of $\mathbf{A}(\mathbf{\Phi})$ are identical. By constructing the STFD matrix from the t-f points of highly localized signal energy, the corresponding signal and noise subspace estimates become more robust to noise than their counterparts obtained using the data covariance matrix [5, 8, 9]. Further, source elimination, rendered through the selection of specific t-f regions, improves DOA estimations.

3. Spatial Polarimetric Time-Frequency Distributions (SPTFDs)

3.1 Polarimetric Modeling

For a far-field transverse electromagnetic (TEM) wave incident on the array, shown in Figure 1, the electric field can be described as

$$\begin{aligned}\vec{E}(t) &= E_\theta(t)\hat{\theta} + E_\phi(t)\hat{\phi} \\ &= [E_\theta(t)\cos(\theta)\cos(\phi) - E_\phi(t)\sin(\phi)]\hat{x} \\ &\quad + [E_\theta(t)\cos(\theta)\sin(\phi) - E_\phi(t)\cos(\phi)]\hat{y} + E_\theta(t)\sin(\theta)\hat{z}\end{aligned} \quad (7)$$

where $\hat{\phi}$ and $\hat{\theta}$ are, respectively, the spherical unit vectors along the azimuth and elevation angles ϕ and θ, viewed from the source. The unit vectors $\hat{x}$, $\hat{y}$ and $\hat{z}$ are defined along the x, y and z directions, respectively. For simplicity and without loss of generality, it is

assumed that the source signal is in the $x-y$ plane, whereas the array is located in the $y-z$ plane. Accordingly, $\theta = 90°$, $\hat{\theta} = -\hat{z}$, and

$$\vec{E}(t) = -E_\phi(t)\sin(\phi)\hat{x} + E_\phi(t)\cos(\phi)\hat{y} + E_\theta(t)\hat{z}. \quad (8)$$

We denote $s(t)$ as the source signal magnitude measured at the receiver reference sensor, with polarization angle $\gamma \in [0,90°]$, and polarization phase difference $\eta \in (-180°,180°]$. The source's vertical and horizontal polarization components, $s^{[v]}(t)$ and $s^{[h]}(t)$, can then be expressed in terms of the respective spherical fields, $E_\theta(t)$ and $E_\phi(t)$, as

$$E_\theta(t) = s^{[v]}(t) = s(t)\cos(\gamma), \quad E_\phi(t) = s^{[h]}(t) = s(t)\sin(\gamma)e^{j\eta}. \quad (9)$$

A signal is referred to as linearly polarized if $\eta = 0°$ or $\eta = 180°$. Substituting Eq. (9) into Eq. (8) results in

$$\vec{E}(t) = s(t)[-\cos(\gamma)\sin(\phi)\hat{x} + \cos(\phi)\sin(\gamma)e^{j\eta}\hat{y} + \cos(\gamma)\hat{z}]. \quad (10)$$

Now we consider that n signals impinge on the array, consisting of m dual-polarized antennas. The vertical and horizontal components of the i th source are expressed as

$$s_i^{[v]}(t) = s_i(t)\cos(\gamma_i) = c_{i1}s_i(t), \quad s_i^{[h]}(t) = s_i(t)\sin(\gamma_i)e^{j\eta_i} = c_{i2}s_i(t), \quad (11)$$

where the parameters $c_{i1} = \cos(\gamma_i)$ and $c_{i2} = \sin(\gamma_i)e^{j\eta_i}$ denote the vertical and horizontal polarization coefficients. The signal received at the l th dual-polarization antenna, with vertical and horizontal antennas located in the $\hat{z}$ and $\hat{y}$ directions, is expressed as

$$\underline{y}_l(t) = [y_l^{[v]}(t), y_l^{[h]}(t)]^T = \sum_{i=1}^{n} [a_{il}^{[v]} \vec{E}_i(t) \cdot \hat{z}, a_{il}^{[h]} \vec{E}_i(t) \cdot \hat{y}]^T = \sum_{i=1}^{n} [a_{il}^{[v]} s_i^{[v]}(t), a_{il}^{[h]} s_i^{[h]}(t) \cos(\phi_i)]^T ,$$

(12)

where $\vec{E}_i(t)$ as the electric field corresponding to the i th signal, $a_{il}^{[v]}$ and $a_{il}^{[h]}$, respectively, are the l th elements of the vertically and horizontally polarized array vectors, $\mathbf{a}^{[v]}(\phi_i)$ and $\mathbf{a}^{[h]}(\phi_i)$, and " $\cdot$ " represents the dot product. It is assumed that the array has been calibrated and both $\mathbf{a}^{[v]}(\phi_i)$ and $\mathbf{a}^{[h]}(\phi_i)$ are known and normalized such that $\left\|\mathbf{a}^{[v]}(\phi_i)\right\|^2 = \left\|\mathbf{a}^{[h]}(\phi_i)\right\|^2 = m$. It is noted that, since the $\cos(\phi_i)$ term is common in all the elements of the horizontally polarized array manifold, it can be absorbed in the array calibration for the region of interest and, therefore, removed from further consideration. Then, the above equation is simplified to

$$\underline{y}_l(t) = [a_{il}^{[v]} s_i^{[v]}(t), a_{il}^{[h]} s_i^{[h]}(t)]^T = s_i(t)\left([a_{il}^{[v]}, a_{il}^{[h]}]^T \circ [c_{i1}, c_{i2}]^T\right) = s_i(t)\mathbf{a}_{il} \circ \mathbf{c}_i , \qquad (13)$$

where the vector

$$\mathbf{c}_i = [c_{i1}, c_{i2}]^T = [\cos(\gamma_i), \sin(\gamma_i) e^{j\eta_i}]^T \qquad (14)$$

represents the polarization signature of the i th signal.

3.2 Polarimetric Time-Frequency Distributions (PTFDs)

For the l th dual-polarized sensor, we define the self- and cross-polarized TFDs, respectively, as

$$D_{x_l^{[i]} x_l^{[j]}}(t, f) = \iint \phi(t-u, \tau) x_l^{[i]}(u + \frac{\tau}{2}) (x_l^{[j]}(u - \frac{\tau}{2}))^* e^{-j2\pi f \tau} du d\tau \qquad (15)$$

and

$$D_{x_l^{[i]}x_l^{[k]}}(t,f) = \iint \phi(t-u,\tau) x_l^{[i]}(u+\frac{\tau}{2})(x_l^{[k]}(u-\frac{\tau}{2}))^* e^{-j2\pi f\tau} du d\tau \,, \qquad (16)$$

where the superscripts i and k denote either v or h. Define

$$\underline{x}_l(t) = [x_l^{[v]}, x_l^{[h]}]^T \,, \qquad (17)$$

to include the two polarization components received in a dual-polarized antenna. Then, the self- and cross-polarized TFDs constitute the 2×2 polarimetric TFD (PTFD) matrix

$$\mathbf{D}_{\underline{x}_l \underline{x}_l}(t,f) = \iint \phi(t-u,\tau) \underline{x}_l(u+\frac{\tau}{2}) \underline{x}_l^H(u-\frac{\tau}{2}) e^{-j2\pi f\tau} du d\tau \,. \qquad (18)$$

The diagonal entries of $\mathbf{D}_{\underline{x}_l \underline{x}_l}(t,f)$ are the self-polarized TFDs $D_{x_l^{[i]}x_l^{[i]}}(t,f)$, whereas the off-diagonal elements are the cross-polarized terms $D_{x_l^{[i]}x_l^{[k]}}(t,f), i \neq k$.

3.3 Spatial Polarimetric Time-Frequency Distributions (SPTFDs)

Equations (12) – (18) correspond to the case of a single dual-polarization sensor. With an array of m dual-polarized antennas, the data vector, for each polarization i, $i = v$ or h, is expressed as

$$\mathbf{x}^{[i]}(t) = [x_1^{[i]}(t), x_2^{[i]}(t), \ldots, x_m^{[i]}(t)]^T = \mathbf{y}^{[i]}(t) + \mathbf{n}^{[i]}(t) = \mathbf{A}^{[i]}(\mathbf{\Phi})\mathbf{s}^{[i]}(t) + \mathbf{n}^{[i]}(t). \qquad (19)$$

Now, we generalize the PTFDs to a multi-sensor receiver. Based on Eq. (19), the following extended data vector can be constructed for both polarizations,

$$\begin{aligned}\mathbf{x}(t) &= \begin{bmatrix}\mathbf{x}^{[v]}(t)\\ \mathbf{x}^{[h]}(t)\end{bmatrix} = \begin{bmatrix}\mathbf{A}^{[v]}(\Phi) & \mathbf{0}\\ \mathbf{0} & \mathbf{A}^{[h]}(\Phi)\end{bmatrix}\begin{bmatrix}\mathbf{s}^{[v]}(t)\\ \mathbf{s}^{[h]}(t)\end{bmatrix} + \begin{bmatrix}\mathbf{n}^{[v]}(t)\\ \mathbf{n}^{[h]}(t)\end{bmatrix}\\ &= \begin{bmatrix}\mathbf{A}^{[v]}(\Phi) & \mathbf{0}\\ \mathbf{0} & \mathbf{A}^{[h]}(\Phi)\end{bmatrix}\begin{bmatrix}\mathbf{Q}^{[v]}\\ \mathbf{Q}^{[h]}\end{bmatrix} + \begin{bmatrix}\mathbf{n}^{[v]}(t)\\ \mathbf{n}^{[h]}(t)\end{bmatrix}\\ &= \mathbf{B}(\Phi)\mathbf{Q}\mathbf{s}(t) + \mathbf{n}(t),\end{aligned} \tag{20}$$

where

$$\mathbf{B}(\Phi) = \begin{bmatrix}\mathbf{A}^{[v]}(\Phi) & \mathbf{0}\\ \mathbf{0} & \mathbf{A}^{[h]}(\Phi)\end{bmatrix} \tag{21}$$

is block-diagonal, and

$$\mathbf{Q} = \begin{bmatrix}\mathbf{Q}^{[v]}\\ \mathbf{Q}^{[h]}\end{bmatrix} \tag{22}$$

is the polarization signature vector of the sources, where

$$\mathbf{q}^{[v]} = [\cos(\gamma_1), \ldots, \cos(\gamma_n)]^T, \quad \mathbf{Q}^{[v]} = \mathrm{diag}(\mathbf{q}^{[v]}), \tag{23}$$

$$\mathbf{q}^{[h]} = [\sin(\gamma_1)e^{j\eta_1}, \ldots, \sin(\gamma_n)e^{j\eta_n}]^T, \quad \mathbf{Q}^{[h]} = \mathrm{diag}(\mathbf{q}^{[h]}). \tag{24}$$

Accordingly,

$$\mathbf{B}(\Phi)\mathbf{Q} = \begin{bmatrix}\mathbf{a}^{[v]}(\phi_1)\cos(\gamma_1) & \ldots & \mathbf{a}^{[v]}(\phi_n)\cos(\gamma_n)\\ \mathbf{a}^{[h]}(\phi_1)\sin(\gamma_1)e^{j\eta_1} & \ldots & \mathbf{a}^{[h]}(\phi_n)\sin(\gamma_n)e^{j\eta_n}\end{bmatrix} = \begin{bmatrix}\tilde{\mathbf{a}}(\phi_1) & \ldots & \tilde{\mathbf{a}}(\phi_n)\end{bmatrix}. \tag{25}$$

The above matrix can be viewed as the extended mixing matrix, with

$$\tilde{\mathbf{a}}(\phi_k) = \begin{bmatrix}\mathbf{a}^{[v]}(\phi_k)\cos(\gamma_k)\\ \mathbf{a}^{[h]}(\phi_k)\sin(\gamma_k)e^{j\eta_k}\end{bmatrix} \tag{26}$$

representing the joint spatio-polarimetric signature of source k.

It is clear that the dual-polarization array, compared to single-polarization case, doubles the vector space dimensionality. Specifically, when $\mathbf{a}^{[v]}(\phi_k) = \mathbf{a}^{[h]}(\phi_k) = \mathbf{a}(\phi_k)$, the above equation simplifies to

$$\tilde{\mathbf{a}}(\phi_k) = \mathbf{a}^{[h]}(\phi_k) \otimes \mathbf{c}_k . \tag{27}$$

It is now possible to combine the polarimetric, spatial, and t-f properties of the source signals incident on the receiver array. The STFD of the dual-polarization data vector, $\mathbf{x}(t)$, can be used in formulating the following SPTFD matrix

$$\mathbf{D}_{\mathbf{xx}}(t,f) = \iint \phi(t-u,\tau)\mathbf{x}(u+\frac{\tau}{2})\mathbf{x}^H(u-\frac{\tau}{2})e^{-j2\pi f\tau}\,du\,d\tau . \tag{28}$$

This SPTFD matrix embodies the information required to address typical problems in array processing, including direction finding, as will be shown in the next section.

When the effect of noise is ignored, the SPTFD matrix is related to the source TFD matrix by the following equation,

$$\mathbf{D}_{\mathbf{xx}}(t,f) = \mathbf{B}(\Phi)\mathbf{Q}\mathbf{D}_{\mathbf{ss}}(t,f)\mathbf{Q}^H\mathbf{B}^H(\Phi) . \tag{29}$$

4. Polarimetric Time-Frequency MUSIC (PTF-MUSIC)

Time-frequency MUSIC (TF-MUSIC) has been recently introduced for improved spatial resolution for signals with clear t-f signatures [7]. It is based on the eigenstructure of the STFD matrix. The PTF-MUSIC is an important generalization of the TF-MUSIC to deal with diversely polarized signals and polarized arrays. It is based on the SPTFD matrix of Eq. (28).

Consider the following spatial signature matrix

$$\mathbf{F}(\phi)=\frac{1}{\sqrt{m}}\begin{bmatrix}\mathbf{a}^{[v]}(\phi) & \mathbf{0}\\ \mathbf{0} & \mathbf{a}^{[h]}(\phi)\end{bmatrix} \tag{30}$$

corresponding to DOA ϕ. Since $\left\|\mathbf{a}^{[i]}(\phi)\right\|^2=m$, $\mathbf{F}^H(\phi)\mathbf{F}(\phi)$ is the 2×2 identity matrix.

To search in the joint spatial and polarimetric domains, we define the following spatio-polarimetric search vector

$$\mathbf{f}(\phi,\mathbf{c})=\frac{\mathbf{F}(\phi)\mathbf{c}}{\left\|\mathbf{F}(\phi)\mathbf{c}\right\|}=\mathbf{F}(\phi)\mathbf{c}, \tag{31}$$

where the vector $\mathbf{c}=[c_1,c_2]^T$ is a unit norm vector with unknown polarization coefficients c_1 and c_2. In Eq. (31), we have used the fact that $\left\|\mathbf{F}(\phi)\mathbf{c}\right\|=[\mathbf{c}^H\mathbf{F}^H(\phi)\mathbf{F}(\phi)\mathbf{c}]^{\frac{1}{2}}=(\mathbf{c}^H\mathbf{c})^{\frac{1}{2}}=1$.

The PTF-MUSIC spectrum is given by the following function [22, 23]

$$P(\phi)=[\min_{\mathbf{c}}\mathbf{f}^H(\phi,\mathbf{c})\mathbf{U}_n\mathbf{U}_n^H\mathbf{f}(\phi,\mathbf{c})]^{-1}=[\min_{\mathbf{c}}\mathbf{c}^H\mathbf{F}^H(\phi)\mathbf{U}_n\mathbf{U}_n^H\mathbf{F}(\phi)\mathbf{c}]^{-1}, \tag{32}$$

where $\mathbf{U}_n$ is the noise subspace obtained from the SPTFD matrix using the selected t-f points. Time-frequency averaging and joint block-diagonalization are two known techniques that can be used to integrate the different STFD or SPTFD matrices constructed from multiple t-f points [5, 7, 25]. The selection of those points from high energy concentration regions pertaining to all or some of the sources enhances the SNR and allows the t-f based MUSIC algorithms to be more robust to noise compared to its conventional MUSIC counterpart [5].

In Eq. (32), the term in brackets is minimized by finding the minimum eigenvalue of the 2×2 matrix $\mathbf{F}^H(\phi)\mathbf{U}_n\mathbf{U}_n^H\mathbf{F}(\phi)$. Thus, a computationally expensive search in the

polarization domain is avoided by performing a simple eigen-decomposition on the 2×2 matrix. As a result, the PTF-MUSIC spectrum can be expressed as

$$P(\phi) = \lambda_{\min}^{-1}[\mathbf{F}^H(\phi)\mathbf{U}_n\mathbf{U}_n^H\mathbf{F}(\phi)], \tag{33}$$

where $\lambda_{\min}[\cdot]$ denotes the minimum eigenvalue operator. The DOAs of the sources are estimated as the locations of the highest peaks in the PTF-MUSIC spectrum. For each angle ϕ_k corresponding to one of the n signal arrivals, $k = 1,2,\ldots,n$, the polarization parameters of the respective source signal can be estimated from

$$\hat{\mathbf{c}}(\phi_k) = \mathbf{v}_{\min}[\mathbf{F}^H(\phi_k)\mathbf{U}_n\mathbf{U}_n^H\mathbf{F}(\phi_k)], \tag{34}$$

where $\mathbf{v}_{\min}[\cdot]$ is the eigenvector corresponding to the minimum eigenvalue $\lambda_{\min}[\cdot]$.

5. Spatio-Polarimetric Correlations

In a conventional single-polarized array problem, the spatial resolution capability of an array highly depends on the correlation between the propagation signatures of the source arrivals [5, 26]. This is determined by the normalized inner product of the respective array manifold vectors. In the underlying problem, in which both the spatial and polarimetric dimensions are involved, the joint spatio-polarimetric correlation coefficient between sources l and k is defined using the extended array manifold $\tilde{\mathbf{a}}(\phi)$, as

$$\begin{aligned}\beta_{l,k} &= \frac{1}{m}\tilde{\mathbf{a}}^H(\phi_k)\tilde{\mathbf{a}}(\phi_l) = \frac{1}{m}\left(c_{k1}^* c_{l1}\left(\mathbf{a}^{[v]}(\phi_k)\right)^H\mathbf{a}^{[v]}(\phi_l) + c_{k2}^* c_{l2}\left(\mathbf{a}^{[h]}(\phi_k)\right)^H\mathbf{a}^{[h]}(\phi_l)\right) \\ &= c_{k1}^* c_{l1}\beta_{l,k}^{[v]} + c_{k2}^* c_{l2}\beta_{l,k}^{[h]}\end{aligned} \tag{35}$$

where $\beta_{l,k}^{[i]} = \frac{1}{m}\left(\mathbf{a}^{[i]}(\phi_k)\right)^H \mathbf{a}^{[i]}(\phi_l)$ is the spatial correlation coefficient between sources l and k for polarization i, with i denoting v or h.

An interesting case arises when the vertically and horizontally polarized array manifolds are identical, i.e., $\mathbf{a}^{[v]}(\phi) = \mathbf{a}^{[h]}(\phi)$. In this case, $\beta_{l,k}^{[v]} = \beta_{l,k}^{[h]}$, and the joint spatio-polarimetric correlation coefficient becomes the product of the individual spatial and polarimetric correlations, that is,

$$\beta_{l,k} = \beta_{l,k}^{[v]} \rho_{l,k} \tag{36}$$

with

$$\rho_{l,k} = \mathbf{c}_k^H \mathbf{c}_l = \cos(\gamma_l)\cos(\gamma_k) e^{j(\eta_l - \eta_k)} + \sin(\gamma_l)\sin(\gamma_k) \tag{37}$$

representing the polarimetric correlation coefficient. In particular, for linear polarizations, $\eta_l = \eta_k = 0$, and Eq. (37) reduces to

$$\rho_{l,k} = \cos(\gamma_l - \gamma_k). \tag{38}$$

Since $|\rho_{l,k}| \le 1$, with the equality holds only when the two sources have identical polarization states, the spatio-polarization correlation coefficient is always equal to or smaller than that of the individual spatial correlation coefficient. The reduction in the correlation value due to polarization diversity, through the introduction of $\rho_{l,k}$, translates to improved distinctions of sources. As such, two sources that could be difficult to resolve using the single-polarized spatial array manifold $\mathbf{a}^{[v]}(\phi)$ or $\mathbf{a}^{[h]}(\phi)$ can be easily separated using the extended spatio-

polarized array manifold, defined by $\tilde{\mathbf{a}}(\phi)$. This improvement is more evident in the case when the source spatial correlation is high, but the respective polarimetric correlation is low.

6. Moving Sources with Time-Varying Polarizations

In this section, we consider the performance of tracking moving targets with time-varying polarization signatures. Time-varying polarizations are often observed when active or passive sources move or change orientations [27]. The performance of polarimetric MUSIC (P-MUSIC) and PTF-MUSIC techniques are discussed and compared. We show that, the SPTFD maintains the instantaneous polarization information at the auto-term t-f points, whereas the energy of desired source signals is localized. Careful treatment of the data samples is, however, required to effectively utilize the polarization diversity, since the construction of the covariance and SPTFD matrices using all available data samples may compromise the polarization distinctions between sources.

Because the SNR enhancement using multi-sensor t-f processing is well documented [5, 6, 9], we consider the noise-free case in this section for notational simplicity. In this case, the received signal vector is

$$\mathbf{x}(t) = \begin{bmatrix} \mathbf{A}^{[v]}(\mathbf{\Phi}(t))(\mathbf{q}^{[v]}(t) \circ \mathbf{s}(t)) \\ \mathbf{A}^{[h]}(\mathbf{\Phi}(t))(\mathbf{q}^{[h]}(t) \circ \mathbf{s}(t)) \end{bmatrix} \tag{39}$$

with $\mathbf{A}^{[i]}(\mathbf{\Phi}(t)) = \left[\mathbf{a}^{[i]}(\phi_1(t)), \ \ldots, \ \mathbf{a}^{[i]}(\phi_n(t))\right], i = v, h$ is the time-varying array response matrix. Note that we used $\mathbf{\Phi}(t) = \left[\phi_1(t), \ \ldots, \ \phi_n(t)\right]$ to emphasize the fact that the DOAs are now time-varying.

6.1 Polarization Diversity and Selection of Data Samples

In order to properly utilize polarization diversity, careful attention should be paid in the selection of data samples. We use the P-MUSIC as the example.

Given the time-varying nature of the source signal polarizations, the covariance matrix of the received signal vector is

$$\mathbf{R}_{xx}(t) = E[\mathbf{x}(t)\mathbf{x}^H(t)] = E\left\{\begin{bmatrix} \mathbf{A}^{[v]}(\Phi(t))(\mathbf{q}^{[v]}(t) \circ \mathbf{s}(t)) \\ \mathbf{A}^{[h]}(\Phi(t))(\mathbf{q}^{[h]}(t) \circ \mathbf{s}(t)) \end{bmatrix} \begin{bmatrix} \mathbf{A}^{[v]}(\Phi(t))(\mathbf{q}^{[v]}(t) \circ \mathbf{s}(t)) \\ \mathbf{A}^{[h]}(\Phi(t))(\mathbf{q}^{[h]}(t) \circ \mathbf{s}(t)) \end{bmatrix}^H \right\}. \tag{40}$$

When the covariance matrix is replaced by using a time average over the entire data samples and considering the special case where the spatial, temporal, and polarimetric signatures can be decoupled, it becomes

$$\begin{aligned} \overline{\mathbf{R}}_{xx} &= \overline{\mathbf{B}} \begin{bmatrix} \overline{\mathbf{q}^{[v]}(t)(\mathbf{q}^{[v]}(t))^H} \circ \overline{\mathbf{R}}_{ss} & \overline{\mathbf{q}^{[v]}(t)(\mathbf{q}^{[h]}(t))^H} \circ \overline{\mathbf{R}}_{ss} \\ \overline{\mathbf{q}^{[h]}(t)(\mathbf{q}^{[v]}(t))^H} \circ \overline{\mathbf{R}}_{ss} & \overline{\mathbf{q}^{[h]}(t)(\mathbf{q}^{[h]}(t))^H} \circ \overline{\mathbf{R}}_{ss} \end{bmatrix} \overline{\mathbf{B}}^H \\ &= \overline{\mathbf{B}} \left\{ \begin{bmatrix} \overline{\mathbf{q}^{[v]}(t)(\mathbf{q}^{[v]}(t))^H} & \overline{\mathbf{q}^{[v]}(t)(\mathbf{q}^{[h]}(t))^H} \\ \overline{\mathbf{q}^{[h]}(t)(\mathbf{q}^{[v]}(t))^H} & \overline{\mathbf{q}^{[h]}(t)(\mathbf{q}^{[h]}(t))^H} \end{bmatrix} \circ \begin{bmatrix} \overline{\mathbf{R}}_{ss} & \overline{\mathbf{R}}_{ss} \\ \overline{\mathbf{R}}_{ss} & \overline{\mathbf{R}}_{ss} \end{bmatrix} \right\} \overline{\mathbf{B}}^H, \end{aligned} \tag{41}$$

where $\overline{\mathbf{R}}_{ss} = \overline{\mathbf{s}(t)\mathbf{s}^H(t)}$, and $\overline{\mathbf{B}} = \begin{bmatrix} \overline{\mathbf{A}^{[v]}(\Phi(t))} & \mathbf{0} \\ \mathbf{0} & \overline{\mathbf{A}^{[h]}(\Phi(t))} \end{bmatrix}$. The time-varying source signal polarization vectors are defined, similarly to Eqs. (23) and (24), as

$$\mathbf{q}^{[v]}(t) = [\cos(\gamma_1(t)), \ldots, \cos(\gamma_n(t))]^T,$$

$$\mathbf{q}^{[h]}(t) = [\sin(\gamma_1(t))e^{j\eta_1(t)}, \ldots, \sin(\gamma_n(t))e^{j\eta_n(t)}]^T.$$

Consider an alternative scenario where the polarimetric signature is time-invariant. Then the covariance matrix can be expressed as

$$\mathbf{R}_{xx}' = \overline{\mathbf{B}}\begin{bmatrix} \mathbf{q}^{[v]}(\mathbf{q}^{[v]})^H & \mathbf{q}^{[v]}(\mathbf{q}^{[h]})^H \\ \mathbf{q}^{[h]}(\mathbf{q}^{[v]})^H & \mathbf{q}^{[h]}(\mathbf{q}^{[h]})^H \end{bmatrix} \circ \begin{bmatrix} \overline{\mathbf{R}}_{ss} & \overline{\mathbf{R}}_{ss} \\ \overline{\mathbf{R}}_{ss} & \overline{\mathbf{R}}_{ss} \end{bmatrix} \overline{\mathbf{B}}^H . \tag{42}$$

The effect of the signal time-varying polarization on the covariance matrix is clear from Eqs. (41) and (42). When $\overline{\mathbf{q}^{[i]}(t)(\mathbf{q}^{[k]}(t))^H} = \mathbf{q}^{[i]}(\mathbf{q}^{[k]})^H$ for $i,k = v,h$, the corresponding covariance matrices are identical, and the two cases of sources with time-varying and time-invariant polarizations will lead to the same performance. Consider, for example, two linearly polarized sources whose polarization angle change linearly over $[0^\circ, 90^\circ]$ for γ_1 and $[90^\circ, 0^\circ]$ for γ_2. The DOAs are assumed time-invariant. This case is equivalent to both sources assuming fixed, time-invariant polarization of $\gamma = 45^\circ$, and thereby, the source polarization diversity cannot be utilized in DOA estimation using P-MUSIC.

To utilize the source signal polarization diversity, the received data covariance matrix in (41) should be constructed using a selected set of data samples (e.g., using moving average of the received data samples) such that the polarization distinction between sources is maintained, even if the source DOAs show insignificant changes over the observation period. In general, for moving target tracking problems, the selection of the data window for the moving average covariance matrix should be determined such that the DOA variation over the window is small.

We maintain, however, that the reduction of data samples may compromise the subspace estimation and, subsequently, DOA estimation performance, particularly when the SNR is relatively low, and/or the sources are closely spaced. The use of t-f representations

overcomes this shortcoming and provides robust subspace estimation in rapidly time-varying polarization environments.

6.2 Polarization Diversity Consideration in PTF-MUSIC

We now show that the instantaneous polarization information is incorporated in the SPTFD and, therefore, PTF-MUSIC maintains polarization diversity, while providing SNR enhancement and source discriminations.

In the presence of time-varying polarized sources, the auto- and cross-polarized SPTFD matrix can be expressed as

$$\begin{aligned}
\mathbf{D}_{\mathbf{x}^{[i]}\mathbf{x}^{[k]}}(t,f) &= \iint \phi(t-u,\tau)\mathbf{x}^{[i]}(u+\frac{\tau}{2})(\mathbf{x}^{[k]}(u-\frac{\tau}{2}))^H e^{-j2\pi f\tau}\,du\,d\tau \\
&= \iint \phi(t-u,\tau)\mathbf{A}^{[i]}(\mathbf{\Phi}(t+\frac{\tau}{2}))\left[(\mathbf{q}^{[i]}(u+\frac{\tau}{2})(\mathbf{q}^{[k]}(u-\frac{\tau}{2}))^H)\circ(\mathbf{s}(u+\frac{\tau}{2})(\mathbf{s}(u-\frac{\tau}{2}))^H)\right]\left(\mathbf{A}^{[k]}(\mathbf{\Phi}(t-\frac{\tau}{2}))\right)^H e^{-j2\pi f\tau}\,du\,d\tau \\
&= \iint \phi(t-u,\tau)\mathbf{A}^{[i]}(\mathbf{\Phi}(t+\frac{\tau}{2}))\left[\mathbf{G}^{[ik]}(u,\tau)\circ\mathbf{K}(u,\tau)\right]\left(\mathbf{A}^{[k]}(\mathbf{\Phi}(t-\frac{\tau}{2}))\right)^H e^{-j2\pi f\tau}\,du\,d\tau
\end{aligned}$$

(43)

where $\mathbf{G}^{[ik]}(t,\tau)=\mathbf{q}^{[i]}(t+\frac{\tau}{2})(\mathbf{q}^{[k]}(t-\frac{\tau}{2}))^H$, and $\mathbf{K}(t,\tau)=\mathbf{s}(t+\frac{\tau}{2})\mathbf{s}^H(t-\frac{\tau}{2})$. When the window length of the applied *t-f* is small,

$$\mathbf{D}_{\mathbf{x}^{[i]}\mathbf{x}^{[k]}}(t,f)\approx\mathbf{A}^{[i]}(\mathbf{\Phi}(t))\mathbf{D}_{\mathbf{s}^{[i]}\mathbf{s}^{[k]}}(t,f)\left(\mathbf{A}^{[k]}(\mathbf{\Phi}(t))\right)^H, \tag{44}$$

where

$$\mathbf{D}_{\mathbf{s}^{[i]}\mathbf{s}^{[k]}}(t,f)=\iint\phi(t-u,\tau)\mathbf{G}^{[ik]}(u,\tau)\circ\mathbf{K}(u,\tau)e^{-j2\pi f\tau}\,du\,d\tau. \tag{45}$$

We assume that the frequency and the polarization signatures of the sources change almost linearly within the temporal span of the t-f kernel. Then, using the first-order Taylor series

expansion, the polarization-dependent terms can be approximated as $\gamma_i(t+\frac{\tau}{2}) = \gamma_i(t)+\frac{\tau}{2}\dot{\gamma}_i(t)$, where $\dot{\gamma}_i(t) = \frac{d}{dt}\gamma_i(t)$. The auto-terms of the source polarization information, which reside on the diagonals of $\mathbf{G}^{[vv]}(t,\tau)$, $\mathbf{G}^{[vh]}(t,\tau)$, $\mathbf{G}^{[hv]}(t,\tau)$ and $\mathbf{G}^{[hh]}(t,\tau)$, are given by

$$\left[\mathbf{G}^{[vv]}(t,\tau)\right]_{ii} = \frac{1}{2}[\cos(2\gamma_i(t)) + \cos(\tau\dot{\gamma}_i(t))] \tag{46}$$

$$\left[\mathbf{G}^{[vh]}(t,\tau)\right]_{ii} = \frac{1}{2}[\sin(2\gamma_i(t)) - \sin(\tau\dot{\gamma}_i(t))] \tag{47}$$

$$\left[\mathbf{G}^{[hv]}(t,\tau)\right]_{ii} = \frac{1}{2}[\sin(2\gamma_i(t)) + \sin(\tau\dot{\gamma}_i(t))] \tag{48}$$

$$\left[\mathbf{G}^{[hh]}(t,\tau)\right]_{ii} = \frac{1}{2}[-\cos(2\gamma_i(t)) + \cos(\tau\dot{\gamma}_i(t))], \tag{49}$$

respectively. The second sinusoidal terms in Eqs. (47) and (48) results in zero values in $\mathbf{D}_{\mathbf{s}^{[i]}\mathbf{s}^{[k]}}(t,f)$ for symmetric t-f kernels. Therefore, $\mathbf{D}_{\mathbf{s}^{[i]}\mathbf{s}^{[k]}}(t,f)$ can be expressed at the auto-term points as

$$D_{s_i^{[v]}s_i^{[v]}}(t,f) = \frac{1}{2}\cos(2\gamma_i(t))D_{s_i s_i}(t,f) + c_{ii}(t,f) \tag{50}$$

$$D_{s_i^{[h]}s_i^{[h]}}(t,f) = -\frac{1}{2}\cos(2\gamma_i(t))D_{s_i s_i}(t,f) + c_{ii}(t,f) \tag{51}$$

$$D_{s_i^{[v]}s_i^{[h]}}(t,f) = D_{s_i^{[h]}s_i^{[v]}}(t,f) = \frac{1}{2}\sin(2\gamma_i(t))D_{s_i s_i}(t,f) \tag{52}$$

with

$$c_{ii}(t,f)=\frac{1}{2}\iint\phi(t-u,\tau)\cos(\tau\dot{\gamma}_i(t))[\mathbf{K}(t,\tau)]_{ii}e^{-j2\pi f\tau}dud\tau. \qquad (53)$$

When different sources are uncorrelated, their t-f signatures have no significant overlap. If the t-f points located in the auto-term region of the ith source are used in constructing the SPTFD matrix, then

$$\mathbf{D}_{xx}(t,f)=\begin{bmatrix}\mathbf{a}^{[v]}(\phi_i(t)) & \mathbf{0}\\ \mathbf{0} & \mathbf{a}^{[h]}(\phi_i(t))\end{bmatrix}\mathbf{M}_i\begin{bmatrix}\mathbf{a}^{[v]}(\phi_i(t)) & \mathbf{0}\\ \mathbf{0} & \mathbf{a}^{[h]}(\phi_i(t))\end{bmatrix}^H \qquad (54)$$

where

$$\mathbf{M}_i=\frac{1}{2}D_{s_is_i}(t,f)\begin{bmatrix}\cos(2\gamma_i(t)) & \sin(2\gamma_i(t))\\ \sin(2\gamma_i(t)) & -\cos(2\gamma_i(t))\end{bmatrix}+\begin{bmatrix}c_{ii}(t,f) & 0\\ 0 & c_{ii}(t,f)\end{bmatrix}. \qquad (55)$$

In the new structure of the SPTFD matrix of Eq. (54), the source time-varying polarization has the effect of loading the diagonal elements with $c_{ii}(t,f)$ and, as such, alters the eigenvalues of the above 2×2 matrix. However, the eigenvectors of $\mathbf{M}_i$ remain unchanged. The new eigenvalues are $\lambda_{i,1,2}=c_{ii}(t,f)\pm\frac{1}{2}D_{s_is_i}(t,f)$. The signal polarization signature, i.e., the eigenvector corresponding to the maximum eigenvalue, is $\mathbf{v}_{i,\max}=[\cos(\gamma_i(t)),\ \sin(\gamma_i(t))]^T$. Therefore, in the context of PTF-MUSIC, the instantaneous polarization characteristics can be utilized for source discriminations.

7. Simulation Results

Two chirp signals are considered and their parameters are listed in Table I. The two sources impinge on a uniform linear array (ULA) of five cross-dipoles with an interelement spacing of half a wave-length. The array responses in both horizontal and vertical

polarizations are identical. The input SNR is 5dB. The source signals' polarization angles ($\gamma_i(t), i = 1,2$) change linearly with time over the observation period of T = 256 samples (Figure 2). Note that sources with polarization angles of 0^o and 180^o are both horizontally polarized, whereas a polarization angle difference of 90^o implies orthogonal polarizations. Figure 3 shows the polarization-averaged pseudo Wigner-Ville distribution (PWVD) of the received data at the reference sensor with a window length of 65. When the sources have low polarization correlation, the cross-terms of the signal components corresponding to the vertical and horizontal polarizations cancel out, resulting in low polarization-averaged cross-term values.

In tracking the moving sources' DOAs, different sets of SPTFD matrices are constructed. Each set uses P consecutive (neighboring) t-f points of the two sources' auto-terms, with the middle t-f point being at t_i. The objective is to examine the proposed algorithm performance at different source polarization states and to demonstrate the tracking accuracy of the algorithm. This is achieved by applying the PTF-MUSIC for each set of SPTFD matrices separately.

Figure 4(a) shows the tracking accuracy of the PTF-MUSIC algorithm for the DOA estimations of the two sources with P=31 and using a PWVD with window length L=65. The performance of P-MUSIC is also shown in Figure 4(b) for P=31 and in Figure 4(c) for P=95. The tracking accuracy of the algorithms was evaluated at 49 time points that are spaced 5 samples apart (i.e., $t_1 = 8$ and $t_{49} = 248$). We note that both techniques use the same data samples. The PTF-MUSIC generally outperforms the P-MUSIC as can be seen in Figure 4. The performance of the PTF-MUSIC is particularly impressive in regions where the signal

energy is highly localized in the t-f domain and the polarization distinction between the two sources is high. The importance of polarization diversity is emphasized by the fact that, in the central and edge regions where the two sources have low polarization distinction, the performance of both PTF-MUSIC and P-MUSIC suffers.

8. Conclusion

This paper considered the application of polarimetric time-frequency (PTF-MUSIC) for tracking moving sources with time-varying polarizations. It has been shown that the difference in the instantaneous polarizations of the sources can be uniquely utilized by the proposed approach to maintain polarization diversity. It is shown that the PTF-MUSIC approach is superior to a covariance matrix approach that is based on a moving window of the received data. The proposed approach also allows for the discrimination of sources based on their time-frequency signal characteristics.

References

[1] L. Cohen, "Time-frequency distributions - a review," *Proc. IEEE*, vol. 77, no. 7, pp. 941-981, July 1989.

[2] S. Qian and D. Chen, *Joint Time-Frequency Analysis – Methods and Applications*, Englewood Cliffs, NJ: Prentice Hall, 1996.

[3] B. Boashash (ed.), *Time-Frequency Signal Analysis and Processing*, Oxford, UK: Elsevier, 2003.

[4] A. Belouchrani and M. G. Amin, "Blind source separation based on time-frequency signal representations," *IEEE Trans. Signal Processing*, vol. 46, no. 11, pp. 2888-2897, Nov. 1998.

[5] Y. Zhang, W. Mu, and M. G. Amin, "Subspace analysis of spatial time-frequency distribution matrices," *IEEE Trans. Signal Processing*, vol. 49, no. 4, pp. 747-759, April 2001.

[6] M. G. Amin, Y. Zhang, G. J. Frazer, and A. R. Lindsey, "Spatial time-frequency distributions: Theory and applications," in L. Debnath (ed.), *Wavelets and Signal Processing*, Boston, MA: Birkhauser, 2003.

[7] A. Belouchrani and M. G. Amin, "Time-frequency MUSIC," *IEEE Signal Processing Letters*, vol. 6, pp. 109-110, May 1999.

[8] M. G. Amin and Y. Zhang, "Direction finding based on spatial time-frequency distribution matrices," *Digital Signal Processing*, vol. 10, no. 4, pp. 325-339, Oct. 2000.

[9] Y. Zhang, W. Mu, and M. G. Amin, "Time-frequency maximum likelihood methods for direction finding," *J. Franklin Inst.*, vol. 337, no. 4, pp. 483-497, July 2000.

[10] A. Hassanien, A. B. Gershman, and M. G. Amin, "Time-frequency ESPRIT for direction-of-arrival estimation of chirp signals," *IEEE Sensor Array and Multichannel Signal Processing Workshop*, Rosslyn, VA, pp. 337–341, Aug. 2002.

[11] W. C. Y. Lee and Y. S. Yeh, "Polarization diversity for mobile radio," *IEEE Trans. Commun.*, vol. COM-20, pp. 912-923, May 1972.

[12] D. Giuli, "Polarization diversity in radars," *Proc. IEEE*, vol. 74, no. 2, pp. 245-269, Feb. 1986.

[13] A. I. Kozlov, L. P. Ligthart, and A. I. Logvin, *Mathematical and Physical Modelling of Microwave Scattering and Polarimetric Remote Sensing*, London, U.K.: Kluwer Academic, 2001.

[14] D. J. McLaughlin, Y. Wu, W. G. Stevens, X. Zhang, M. J. Sowa, and B. Weijers, "Fully polarimetric bistatic radar scattering behavior of forested hills," *IEEE Trans. Antennas Propagat.*, vol. 50, no. 2, pp. 101-110, Feb. 2002.

[15] F. Sadjadi, "Improved target classification using optimum polarimetric SAR signatures," *IEEE Trans. Aerosp. Electron. Syst.*, vol. 38, no. 1, pp. 38-49, Jan. 2002.

[16] A. L. Pazmany, R. E. McIntosh, R. D. Kelly, and G. Vali, "An airborne 95 GHz dual-polarized radar for cloud studies," *IEEE Trans. Geoscience and Remote Sensing*, vol. 32, no. 4, pp. 731-739, July 1994.

[17] S. H. Yueh, W. J. Wilson, and S. Dinardo, "Polarimetric radar remote sensing of ocean surface wind," *IEEE Trans. Geoscience and Remote Sensing*, vol. 40, no. 4, pp. 793-800, April 2002.

[18] G. A. Ioannidids and D. E. Hammers, "Optimum antenna polarizations for target discrimination in clutter," *IEEE Trans. Antennas Propagat.*, vol. AP-27, pp. 357-363, 1979.

[19] D. A. Garren, A. C. Odom, M. K. Osborn, J. S. Goldstein, S. U. Pillai, and J. R. Guerci, "Full polarization matched-illumination for target detection and identification," *IEEE Trans. Aerosp. Electron. Syst.,* vol. 38, no. 3, pp. 824-837, July 2002.

[20] E. R. Ferrara and T. M. Parks, "Direction finding with an array of antennas having diverse polarizations," *IEEE Trans. Antennas Propagat.,* vol. 31, pp. 231-236, March 1983.

[21] J. Li and R. J. Compton, "Angle and polarization estimation using ESPRIT with a polarization sensitive array," *IEEE Trans. Antennas Propagat.,* vol. 39, pp. 1376-1383, Sept. 1991.

[22] Y. Zhang, M. G. Amin, and B. A. Obeidat, "Polarimetric array processing for nonstationary signals," in S. Chandran (ed.), *Adaptive Antenna Arrays: Trends and Applications*, Berlin, Germany: Springer-Verlag, 2004.

[23] Y. Zhang, B. A. Obeidat, and M. G. Amin, "Spatial polarimetric time-frequency distributions for direction-of-arrival estimations," *IEEE Trans. Signal Processing* (in press).

[24] B. A. Obeidat, Y. Zhang, and M. G. Amin, "Polarimetric time-frequency ESPRIT," *Ann. Asilomar Conf. Signals, Sys., and Comput.*, Pacific Grove, CA, Nov. 2003.

[25] A. Belouchrani, M. G. Amin, and K. Abed-Meraim, "Direction finding in correlated noise fields based on joint block-diagonalization of spatio-temporal correlation matrices," *IEEE Signal Processing Letters*, vol. 4, no. 9, pp. 266-268, Sept. 1997.

[26] P. Stoica and A. Nehorai, "MUSIC, maximum likelihood and Cramer-Rao bound," *IEEE Trans. Acoust., Speech, and Sig. Proc.*, vol. 37, no. 5, pp. 720-741, May 1989.

[27] Y. Zhang and M. G. Amin, "Joint Doppler and polarization characterization of moving targets," *IEEE AP-S Int. Symp.*, Monterey, CA, June 2004.

Table I. Signal parameters of moving sources with time-varying polarizations

	Start freq.	End Freq.	DOA (deg.)	γ (deg.)	η (deg.)
Source 1	0	0.20	-15 to 5	0 to 180	0
Source 2	0.20	0.40	-10 to 10	180 to 0	0

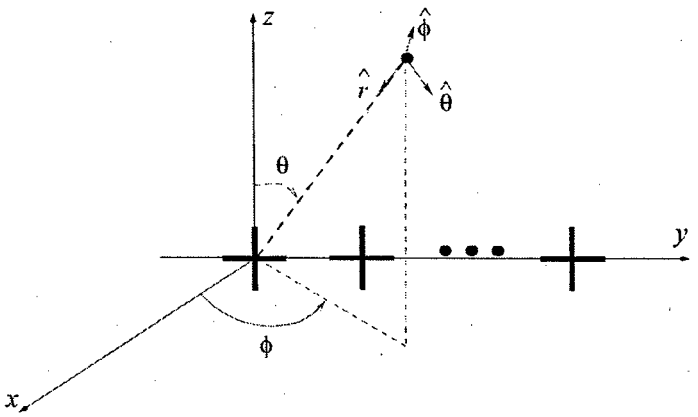

Figure 1. Dual-polarized array.

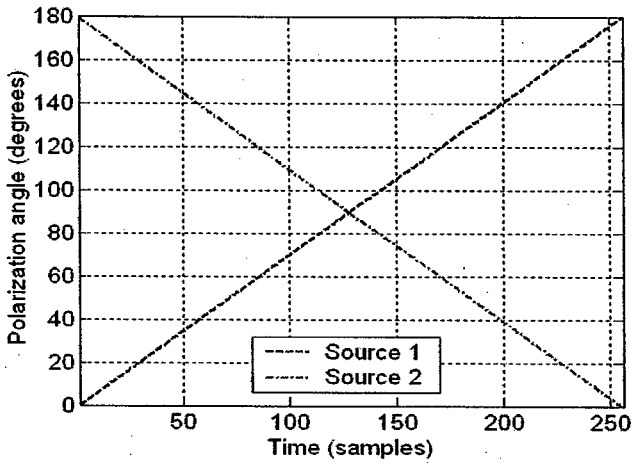

Figure 2. Time-varying polarization signatures.

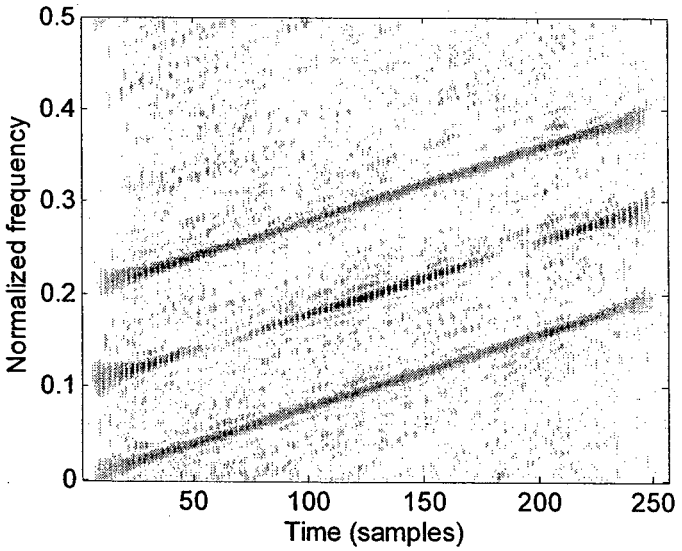

Figure 3. Polarization-averaged PWVD of the received data at the reference sensor.

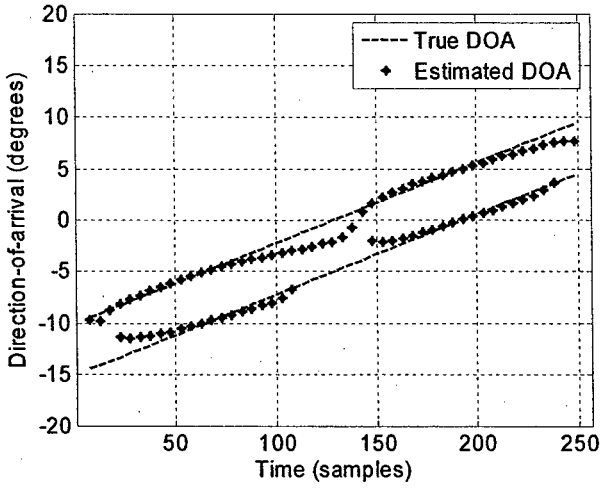

(a) PTF-MUSIC (using 31 time-frequency points)

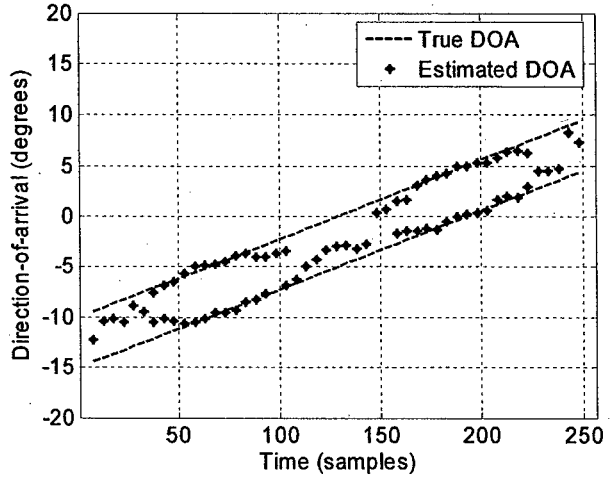

(b) P-MUSIC (using 31 data samples)

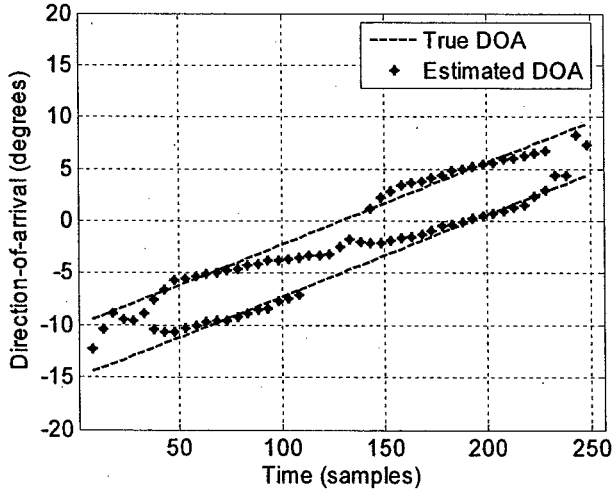

(c) P-MUSIC (using 95 data samples)

Figure 4. PTF-MUSIC and P-MUSIC tracking performance.

DOA and Polarization Estimation for Wideband Sources

Baha A. Obeidat, Yimin Zhang, and Moeness G. Amin

Abstract

This paper presents an approach to direction-of-arrival (DOA) and polarization estimations of far-field wideband signals using an array of cross-polarized dual-feed sensors. The wideband signals are decomposed into a set of narrowband signals. Coherent signal subspace processing is then applied to dimension-extended source signal correlation matrices at different narrowband frequencies, leading to the construction of single signal subspace. The utilization of polarization diversity through the use of a dual-feed cross-polarized array to process the polarized signal arrivals lends an additional degree of freedom, leading to performance improvement over the case where a single-polarization array is used.

I. Introduction

Direction-of-arrival (DOA) estimation for far-field sources has been the subject of numerous array processing studies [1] [2]. When the signals that are incident on an array are wideband, coherent signal subspace processing [3] can be used to apply typically narrowband subspace-based estimation methods to the wideband case. Coherent signal subspace processing relies on the frequency domain decomposition of the array output into a number of narrowband outputs to which the conventional narrowband array processing model applies. For each frequency subband, transformation matrices are designed that focus their respective covariance matrices to a particular frequency of interest. The covariance matrices are later coherently combined to produce a coherent signal space [4]. This approach outperforms its non-coherent counterpart.

Polarization and polarization diversity, on the other hand, have been used in wireless communication systems [5] [6] and in various types of radar systems [7]. Additionally, they have been incorporated into array processing for DOA estimation for narrowband sources [8]. The incorporation of signal polarization information lends an additional degree of freedom and consequently results in improved DOA estimation and signal synthesis [9] [10].

This paper considers the estimation of DOA and polarization signatures of wideband sources. We show that the coherent subspace processing remains effective in dual-polarization applications. Because the array manifold in one polarization may differ to that of the other polarization, the transformation matrices in general should be design separately for different polarizations. The use of polarization diversity is particularly effective when the source signals are closely spaced but have distinct polarizations. Simulation results are provided which show the superior performance of the proposed method in comparison to single-polarized arrays with identical as well as extended apertures.

II. Signal Model

A. Signal Model

Consider an M-element array of identical cross-polarized (such as horizontal and vertical), dual-feed sensors as shown in Fig. 1. The vertically polarized sensors are placed in

the z-axis and the horizontally polarized sensors are placed in the y-axis. Upon the array N polarized farfield wideband sources are incident. It is assumed that the source signals lie in the x-y plane such that their elevation angles, θ_n are 90 degrees and their azimuth angles are denoted as $\phi_n, n = 1, 2, \ldots, N$. The source signals are assumed to have fixed polarizations over the observation period. Additionally, since the sources are farfield, it is practical to assume that the source signal polarizations do not change as received by one sensor to the next.

The received data across the M vertically polarized sensors is converted to baseband, time-sampled as

$$\mathbf{x}^{[v]}(t) = \mathbf{A}^{[v]}(t)\mathbf{s}^{[v]}(t) + \mathbf{n}^{[v]}(t) \tag{1}$$

with the array response matrix as

$$\mathbf{A}^{[v]}(t) = \left[\mathbf{a}^{[v]}(\phi_1, t) \quad \ldots \quad \mathbf{a}^{[v]}(\phi_N, t)\right] \tag{2}$$

where $\mathbf{a}^{[v]}(\phi_n, t)$ denotes the array response vector for the nth source signal. $\mathbf{n}^{[v]}(t)$ is the temporal domain additive sensor noise vector. The received signal vector in the vertical polarization is $\mathbf{s}^{[v]}(t)$ which can be decomposed as $\mathbf{s}^{[v]}(t) = \mathbf{Q}^{[v]}\mathbf{s}(t)$ since the source polarization is constant over the observation period and independent of the frequency. $\mathbf{s}(t)$ is now the polarization-free received signal vector and the matrix containing the source signal vertical polarization components as

$$\mathbf{Q}^{[v]} = \text{diag}[\cos(\gamma_1), \quad \ldots \ , \ \cos(\gamma_N)]. \tag{3}$$

Then, (1) can be rewritten as

$$\mathbf{x}^{[v]}(t) = \mathbf{A}^{[v]}(t)\mathbf{Q}^{[v]}\mathbf{s}(t) + \mathbf{n}^{[v]}(t) \tag{4}$$

The output of the array is then frequency decomposed into J nonoverlapping complex subband components. The bandwidth of each subband is much smaller than its central frequency $f_j, j = 1, 2, \ldots, J$, so that each subband snapshot approximately satisfies the classical narrowband assumption [4]. The kth, $k = 1, 2, \ldots, K$, vertically polarized snapshot received signal vector follows the narrowband model and is written as

$$\mathbf{x}_k^{[v]}(f_j) \ = \ \mathbf{A}^{[v]}(f_j)\mathbf{Q}^{[v]}\mathbf{s}_k(f_j) + \mathbf{n}_k^{[v]}(f_j) \tag{5}$$

where

$$\mathbf{A}^{[v]}(f_j) = [\mathbf{a}_1^{[v]}(\phi_1, f_j), \ldots, \mathbf{a}_N^{[v]}(\phi_N, f_j)] \tag{6}$$

is the vertical array response matrix for the frequency f_j and polarization with $\mathbf{a}_n^{[v]}(\phi_n, f_j)$ as the vertical array response of the nth source at the jth frequency. $\mathbf{n}_k^{[v]}(f_j)$ is the $M \times 1$ noise vector in the vertical polarization at kth sample of the frequency f_j. $\mathbf{s}_k(f_j)$ is the polarization-free source signal vector at frequency f_j.

The same type of manipulation can be applied to the received signal across the horizontally polarized array to yield

$$\mathbf{x}_k^{[h]}(f_j) = \mathbf{A}^{[h]}(f_j)\mathbf{Q}^{[h]}\mathbf{s}_k(f_j) + \mathbf{n}_k^{[h]}(f_j), \tag{7}$$

with

$$\mathbf{Q}^{[h]} = \text{diag}[\sin(\gamma_1)e^{j\eta_1}, \ \ldots \ , \sin(\gamma_N)e^{j\eta_N}] \tag{8}$$

Concatenating the received signal in the horizontal and vertical polarizations provides the extended-dimension received signal vector,

$$\mathbf{x}_k(f_j) \ = \ \begin{bmatrix} \mathbf{x}_k^{[v]}(f_j) \\ \mathbf{x}_k^{[h]}(f_j) \end{bmatrix} = \begin{bmatrix} \mathbf{A}^{[v]}(f_j)\mathbf{Q}^{[v]}\mathbf{s}_k(f_j) \\ \mathbf{A}^{[h]}(f_j)\mathbf{Q}^{[h]}\mathbf{s}_k(f_j) \end{bmatrix} + \begin{bmatrix} \mathbf{n}_k^{[v]}(f_j) \\ \mathbf{n}_k^{[h]}(f_j) \end{bmatrix}. \tag{9}$$

III. Proposed Method

The idea of coherent signal subspace was first proposed in [3]. When $\mathbf{A}^{[i]}(f_j)$, $i = v$ or h, $j = 1, 2, \ldots, J$, are full rank, one can design the transformation matrices, $\mathbf{T}^{[i]}(f_j)$, such that

$$\mathbf{T}^{[i]}(f_j)\mathbf{A}^{[i]}(f_j) = \mathbf{A}^{[i]}(f_0). \tag{10}$$

In the underlying dual-polarization scenario, it can be cast in a block diagonal form to give

$$\mathbf{T}(f_j) \begin{bmatrix} \mathbf{A}^{[v]}(f_j) \\ \mathbf{A}^{[h]}(f_j) \end{bmatrix} \ \triangleq \ \begin{bmatrix} \mathbf{T}^{[v]}(f_j) & \mathbf{0} \\ \mathbf{0} & \mathbf{T}^{[h]}(f_j) \end{bmatrix} \begin{bmatrix} \mathbf{A}^{[v]}(f_j) \\ \mathbf{A}^{[h]}(f_j) \end{bmatrix} = \begin{bmatrix} \mathbf{A}^{[v]}(f_0) \\ \mathbf{A}^{[h]}(f_0) \end{bmatrix}. \tag{11}$$

Generally, since the array responses in the vertical and horizontal polarization may be different, the two focusing matrices are designed to focus the array response matrix in the vertical or horizontal polarizations to the frequency of interest.

Applying the block diagonal transformation matrix to the extended-dimension received signal vector will yield

$$\mathbf{y}(f_j) = \mathbf{T}(f_j)\mathbf{x}(f_j) \tag{12}$$

from which a new covariance matrix can be constructed

$$\begin{aligned}
\mathbf{R}_{\mathbf{yy}} &= \sum_{j=1}^{J} \mathbf{T}(f_j)\mathbf{x}(f_j)\left(\mathbf{T}(f_j)\mathbf{x}(f_j)\right)^H \\
&= \begin{bmatrix} \mathbf{A}^{[v]}(f_0)\mathbf{Q}^{[v]} \\ \mathbf{A}^{[h]}(f_0)\mathbf{Q}^{[h]} \end{bmatrix} \sum_{j=1}^{J} \mathbf{R}_{\mathbf{ss}}(f_j) \begin{bmatrix} \mathbf{A}^{[v]}(f_0)\mathbf{Q}^{[v]} \\ \mathbf{A}^{[h]}(f_0)\mathbf{Q}^{[h]} \end{bmatrix}^H + \sigma^2 \sum_{j=1}^{J} \mathbf{T}(f_j)\mathbf{P}(f_j)\mathbf{T}^H(f_j) \\
&\triangleq \begin{bmatrix} \mathbf{A}^{[v]}(f_0)\mathbf{Q}^{[v]} \\ \mathbf{A}^{[h]}(f_0)\mathbf{Q}^{[h]} \end{bmatrix} \mathbf{R}'_{\mathbf{ss}} \begin{bmatrix} \mathbf{A}^{[v]}(f_0)\mathbf{Q}^{[v]} \\ \mathbf{A}^{[h]}(f_0)\mathbf{Q}^{[h]} \end{bmatrix}^H + \sigma^2\mathbf{P}'.
\end{aligned} \tag{13}$$

where

$$\mathbf{R}'_{\mathbf{ss}} = \sum_{j=1}^{J} \mathbf{R}_{\mathbf{ss}}(f_j) \tag{14}$$

and

$$\mathbf{P}' = \sum_{j=1}^{J} \mathbf{T}(f_j)\mathbf{P}(f_j)\mathbf{T}^H(f_j) \tag{15}$$

A. Spatio-polarimetric correlations

It is evident from (13) that the array has a extended-dimension aperture. In this structure, the closeness of two sources, l and m, is determined by their spatio-polarimetric correlation coefficient. Consider a simple scenario where the array responses at the focusing frequency are identical in both polarizations, i.e. $\mathbf{a}^{[v]}(\phi, f_0) = \mathbf{a}^{[h]}(\phi, f_0) = \mathbf{a}(\phi, f_0)$, the spatio-polarimetric correlation coefficient is defined as the product of the spatial correlation coefficient and the polarimetric correlation coefficient [11], that is

$$\tilde{\beta}_{m,l} = \beta_{m,l}\rho_{l,m}. \tag{16}$$

In (21), the spatial correlation coefficient is the normalized inner product of the sources' array responses at the focusing frequency,

$$\beta_{m,l} = \frac{1}{M}\mathbf{a}_m^H(\phi, f_0)\mathbf{a}_l(\phi, f_0), \tag{17}$$

and their respective polarimetric correlation coefficient is

$$\rho_{m,l} = \cos(\gamma_l)\cos(\gamma_m)e^{j(\eta_l - \eta_m)} + \sin(\gamma_l)\sin(\gamma_m). \tag{18}$$

In particular when the soruces are linearly polarized, $\eta_n = 0, n = 1, 2, \ldots, N$, (19) is simplified as

$$\rho_{m,l} = \cos(\gamma_l \pm \gamma_m). \tag{19}$$

When an M-element array of non-polarization sensitive sensors is used, the spatial correlation coefficient between two source incident upon it is merely $\beta_{m,l}$. Since $|\rho_{m,l}| \leq 1$, the use of a dual-polarized array can only reduce the spatio-polarimetric correlation coefficient. The reduction is particularly significant when the sources are closely spaces but have distinct polarizations.

A $2M$-element array of equally spaced non-polarization sensitive sensors will have a spatial correlation of

$$\hat{\beta}_{m,l} = \beta_{m,l}\hat{\rho}_{l,m}, \tag{20}$$

where $\hat{\rho}_{l,m}$ is the reduction is in the spatial correlation caused by the doubling the number of sensors and extending the array aperture. This coefficient is

$$|\hat{\rho}_{l,m}| = \cos\left[\pi M \frac{d}{\lambda_0}(\sin\phi_l - \sin\phi_m)\right], \tag{21}$$

where λ_0 is the wavelength of the focusing frequency.

B. Polarimetric MUSIC

The coherent signal subspace, $\mathbf{E}_s = \left[\mathbf{e}_1, \ \ldots \ , \ \mathbf{e}_N\right]$, of dimension $2M \times N$ is constructed from the eigenvectors corresponding to the N largest eigenvalues of $\mathbf{R_{yy}}$. The noise subspace, on the other hand, is constructed using the smallest $2M-N$ and is denoted $\mathbf{E}_n$. The polarimetric MUSIC spectrum is given by

$$P(\phi) = \frac{1}{\lambda_{\min}[\mathbf{B}^H(\phi, f_0)\mathbf{E}_n\mathbf{E}_n^H\mathbf{B}(\phi, f_0)]} \tag{22}$$

where $\lambda_{\min}$ denotes the minimum eigenvalue operator and

$$\mathbf{B}(\phi, f_0) = \begin{bmatrix} \mathbf{a}^{[v]}(\phi, f_0) & \mathbf{0} \\ \mathbf{0} & \mathbf{a}^{[h]}(\phi, f_0) \end{bmatrix} \tag{23}$$

is the dual-polarization search matrix at the focusing frequency f_0.

The DOAs of the sources are estimated as the locations of the highest peaks in the MUSIC spectrum. For each angle ϕ_n, $n = 1, \ldots, N$, the polarization parameters of the respective source signal can be estimated from

$$\hat{\mathbf{c}}(\phi_n) \;=\; \mathbf{v}_{\min}[\mathbf{B}^H(\phi, f_0)\mathbf{E}_n\mathbf{E}_n^H\mathbf{B}(\phi, f_0)], \tag{24}$$

where $\mathbf{v}_{\min}[\cdot]$ is the eigenvector corresponding to the minimum eigenvalue $\lambda_{\min}[\cdot]$.

IV. Simulations

A four-sensor uniform linear cross-polarized array is considered with each sensor consisting of a pair of horizontally and vertically polarized elements. The array has identical responses in the horizontal and vertical directions. The interelement spacing is half of the wavelength at the focusing frequency, $f_0 = 100$ Hz. Two farfield sources with DOAs of $\phi_1 = 10°$ and $\phi_2 = 11°$ impinge on the array with polarization angles $\gamma_1 = 45°$ and $\gamma_2 = -45°$, respectively. The two sources are linearly polarized, i.e., their polarizations phase angles $\eta_1 = \eta_2 = 0°$. The two sources have the same central frequency, $f_0 = 100$ Hz, and a bandwidth of 40 Hz. The SNR is set to 0dB, and the number of frequency subbands used was $J = 33$ with each of $K = 100$ snapshots. The search grid used for the MUSIC and polarimetric MUSIC methods was 0.01°. The performance of the polarimetric MUSIC is compared to that of the conventional MUSIC using a similar array with horizonal polarized sensors in place of the cross-polarized sensors.

Since the dual-polarized requires twice the processing as that of a non-polarized array with 4 sensors, a fairer comparison would be against that of an array with twice the number of sensors, i.e., 8 sensors. For this purpose we also performed simulations to examine the performance of the proposed method when compared to that of a non-polarized array and that of a non-polarized uniform linear array with twice the number of sensors. It is worth noting, however, that the 8-element array uses more than twice the aperture as that of the dual-polarized array used since both has the same interelement spacing. In fact, the dual-polarized array's aperture is $\frac{3c}{2f_0}$, while the 8-element array has an aperture of $\frac{7c}{2f_0}$.

Figure 2 shows a single trial run of the spatial spectra. Note that in this case the two sources have orthogonal polarizations and, irrespective of the spatial separation of

the sources, the joint spatio-polarimetric correlation coefficient between the two sources is zero. As a result, while the conventional MUSIC cannot resolve the two closely spaced sources, the polarimetric MUSIC provides accurate DOA estimations.

Figure 3 shows the root mean squared error (RMSE) performance of the DOA estimation of the three types of arrays. The results are obtained from 100 independent trials. It is evident that the polarimetric methods outperforms the two other methods. In this example the spatial correlation coefficient between the two source is $\beta_{1,2} = 0.9982$, a high value due to their close spatial separation. However, the polarimetric correlation coefficient was $\rho_{1,2} = 0$ due to the fact that the two sources are orthogonal in polarization. That reduces the spatial polarimetric correlation to the product of the two, i.e., zero. As for the 8-element array, the spatial correlation it its case is $\tilde{\beta}_{1,2} = 0.9924$ which remains a high value. The difference in the spatial correlation or the spatial polarimetric correlation can explain the difference in the performance of the three methods.

When the polarization angle of source 1 is $\gamma_1 = 30$ and that of source 2 is $\gamma_1 = 60$, whereas all other variables remain unchanged, the performance of the three types of arrays is compared in Fig. 4. Here the polarimetric correlation coefficient between the two sources is $\rho_{1,2} = 0.866$ which results in a spatio-polarimetric correlation coefficient of 0.8644 as opposed to 0 in the previous set. The performance of the polarimetric MUSIC worsens but outperforms that os the other types of arrays. As in other polarimetric-based methods, the performance of this method in DOA estimation is a function of the polarization diversity among the source signals. The higher the polarization diversity the better the performance.

V. Conclusion

This paper proposes a direction-of-arrival (DOA) estimation method for wideband polarized farfield sources that are incident on an array of cross-polarized double-feed sensors. This method utilizes the received signal across the array's two polarization arms to construct a dimension extended received signal vector. Matrix focusing is then used for the purpose of constructing a coherent signal subspace. When the source signals have diverse polarizations this method is shown to outperform the conventional non-polarimetric method.

References

[1] R. O. Schmidt, "Multiple emitter location and signal parameter estimation," *IEEE Trans. Antennas Propagat.*, vol. 34, no. 3, pp. 276–280, March 1986.

[2] F. C. Schweppe, "Sensor-array data processing for multiple-signal sources," *IEEE Trans. Inform. Theory* vol. 14, no. 2, pp. 294-305, March 1968.

[3] H. Wang and M. Kaveh, "Coherent signal-subspace processing for the detection and estimation of angles of arrival of multiple wide-band sources," *IEEE Trans. Acoust., Speech, Signal Processing*, vol. 33, no. 4, pp. 823–831, Aug. 1985.

[4] E. D. DiClaudio and R. Parisi, "WAVES: Weighted average of signal subspaces for robust wideband direction finding," *IEEE Trans. Signal Processing*, vol. 49, No. 10, pp. 2179–2191, Oct. 2001.

[5] R. U. Nabar, H. Bolcskei, V. Erceg, D. Gesbert, A. J. Paulraj, "Performance of multiantenna signaling techniques in the presence of polarization diversity," *IEEE Trans. Signal Processing*, vol. 50, No. 10, pp. 2553–2562, Oct. 2002.

[6] W. C. Y. Lee and Y. S. Yeh, "Polarization diversity for mobile radio," *IEEE Trans. Commun.*, vol. COM-20, pp. 912–923, May 1972.

[7] D. Giuli, "Polarization diversity in radars," *Proc. IEEE*, vol. 74, no. 2, pp. 245–269, Feb. 1986.

[8] E. R. Ferrara and T. M. Parks, "Direction finding with an array of antennas having diverse polarizations," *IEEE Trans. Antennas Propagat.*, vol. 31, pp. 231–236, March 1983.

[9] M. G. Amin and Y. Zhang, "Bilinear signal synthesis using polarization diversity," *IEEE Signal Processing Letters*, vol. 11, no. 3, pp. 338–340, March 2004.

[10] Y. Zhang, M. G. Amin, and B. A. Obeidat, "The spatial polarimetric time-frequency distributions and their applicaiton to direction-of-arrival estimation," *Proc. SPIE*, vol. 5205, Aug. 2003.

[11] Y. Zhang and M. G. Amin, "Spatial and polarization correlations in array processing," *IEEE Sensor Array and Multichannel Signal Processing Workshop*, Barcelona, Spain, July 2004.

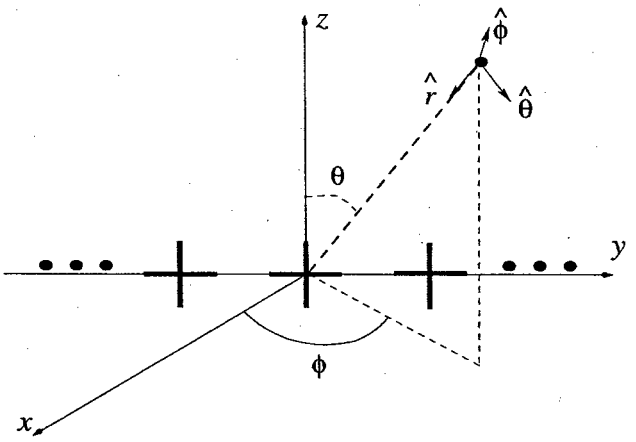

Fig. 1. Dual-polarized array.

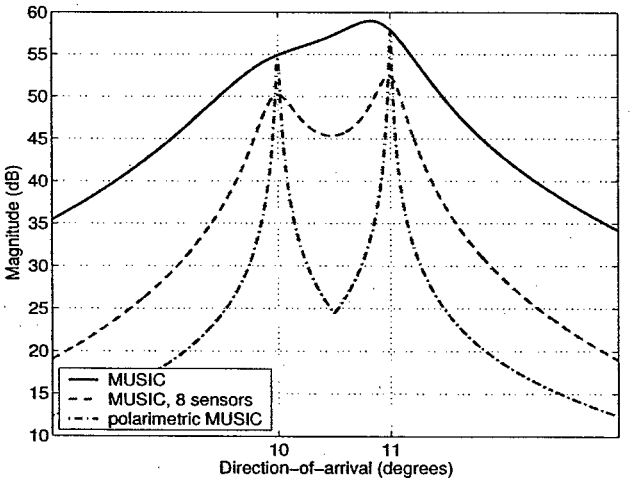

Fig. 2. Polarimetric MUSIC and MUSIC spectra.

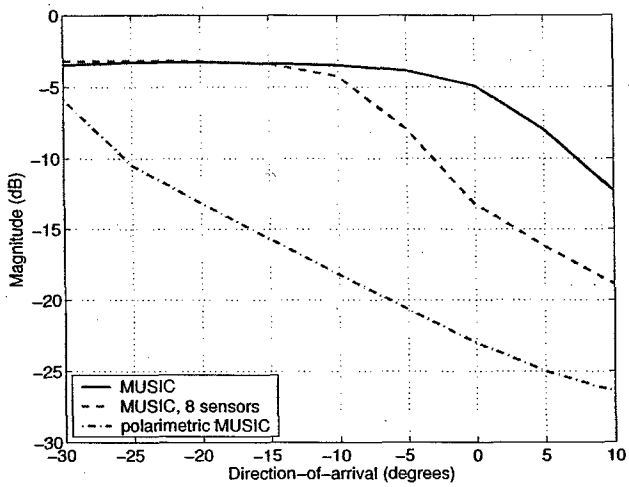

Fig. 3. RMSE of the DOA estimation.

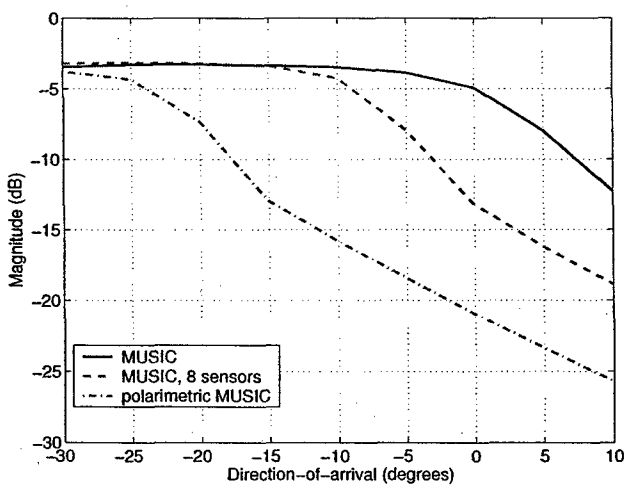

Fig. 4. RMSE of the DOA estimation.

Sensor Configuration in Polarized Antenna Arrays

Baha A. Obeidat, Moeness G. Amin, Yimin Zhang, and Ahmad Hoorfar

Abstract

Single- and dual-polarized array configurations are often used in imaging and radar applications. In this paper, spatio-polarimetric correlation are used as a framework to evaluate the direction finding performance of different receiver configurations employing double-feed dual-polarized array as well as arrays of single-feed single-polarized elements. The spatio-polarimetric correlation coefficients are derived for several array reconfigurations and used to provide a configuration-based performance comparison based on spatial resolution and grating lobes.

I. Introduction

It is well known that the use of dual polarizations can enhance the performance of direction-of-arrival (DOA) estimation in array processing [1], [2], [3] and improve robustness to channel fading in wireless communications [4].

Many of modern communication and radar systems employ antenna arrays made of microstrip or other printed radiating elements. These antenna elements have many advantages, including low profile, lightweight, easy integration to various shapes and surfaces and low-production cost. One main disadvantage of microstrip patch antenna, however, is its narrow bandwidth. Over the years, many techniques have been reported in the literature for bandwidth enhancement of these low-profile antennas [5]. Extension of such wideband techniques to design of dual-polarized dual-feed low-profile antennas, however, is not straightforward if one also requires low polarization isolation between the two output (input) ports, which is often the case in many sensitive applications. In fact, a typical polarization isolation constraint of less than 25dB drastically reduces the operating bandwidth. One possible solution to avoid the polarization isolation issue, and the associated complexity of two-port elements in a large array scenario, is to use a wideband linearly polarized single-port antenna that also senses the orthogonal polarization by a 90^{o} mechanical rotation of the antenna element using a motor-driven turntable. Another alternative solution may be the use of active elements, e.g., varactor or pin diodes, to control and switch between the two states of polarization of a wideband dual-polarized antenna element [6].

Therefore, the capability to reconfigure a double-feed dual-polarized array into a simplified array of single-feed single-polarized sensors becomes of particular interest to array processing for polarized signals. The motivation to simplify the array structure in hardware stems from the fact that single polarized antennas and antenna arrays are more commercially available than the dual-polarized double-feed arrays. Also, with the capability to change the sensor polarizations within the array it becomes important to compare the performance of a dual-polarized array with its single-polarized sensor reconfigurations.

In this paper, we compare the performance of a double-feed dual-polarized array to other affiliate reconfigurations consisting of single-feed single-polarized antenna elements.

Of interest are two array reconfigurations; a reconfigured array of all vertical polarized antennas which is concatenated with an array of all horizontal polarizations, and a reconfigured array of alternating vertical and horizontal polarizations. The spatio-polarimetric correlation coefficients and the DOA estimation are used to assess the performance of the array reconfigurations.

II. Signal Model

Assume L source signals $s_l(t), l = 1, ..., L$, are incident on an array of N dual-polarized antenna sensors. We use $^{[v]}$ and $^{[h]}$ to represent the orthogonal vertical and horizontal polarizations at each sensor. The received data for each polarization is the linear combination of the same source polarization components and noise. That is, the signal received at the nth sensor of polarization i, $i = v$ or h, is

$$x_n^{[i]}(t) = \sum_{l=1}^{L} a_{n,l}^{[i]} s_l^{[i]}(t) + n_n^{[i]}(t), \tag{1}$$

where $a_{n,l}^{[i]}$ represents the propagation coefficient of the lth source with polarization i, $s_l^{[i]}(t)$, to the nth array sensor, and $n_n^{[i]}(t)$ is the noise component at the same polarization.

The data vector at each polarization, $\mathbf{x}^{[i]}(t)$, $i = v$ or h, is expressed as

$$\begin{aligned} \mathbf{x}^{[i]}(t) &= \mathbf{y}^{[i]}(t) + \mathbf{n}^{[i]}(t) \\ &= \mathbf{A}^{[i]}\mathbf{s}^{[i]}(t) + \mathbf{n}^{[i]}(t) \\ &= \mathbf{A}^{[i]}\mathbf{P}^{[i]}\mathbf{s}(t) + \mathbf{n}^{[i]}(t), \end{aligned} \tag{2}$$

where $\mathbf{y}^{[i]}(t)$ and $\mathbf{n}^{[i]}(t)$ are, respectively, the noise-free data vector and the noise vector, $\mathbf{A}^{[i]} = [\mathbf{a}_1^{[i]}, \cdots, \mathbf{a}_L^{[i]}]$ is the data mixing matrix, and $\mathbf{s}^{[i]}(t)$ is a vector representing the ith polarization components of the source signal vector, $\mathbf{s}(t)$. In addition, the polarization information can be decoupled from the source waveform and separately captured in matrix $\mathbf{P}^{[i]} = \text{diag}[p_1^{[i]}, \cdots, p_L^{[i]}]$, where

$$p_l^{[v]} = \cos(\gamma_l) \quad \text{and} \quad p_l^{[h]} = \sin(\gamma_l)e^{j\eta_l} \tag{3}$$

are the coefficients of the lth source projected on the v and h polarizations. In (3), $\gamma_l \in [0, \frac{\pi}{2}]$ is the polarization angle that determines the magnitude ratio between the

two polarizations, whereas $\eta_l \in (-\pi, \pi]$ is the phase difference between the two polarizations. In this paper we only consider linearly polarized signals, i.e., $\eta_l = 0$, $l = 1, \ldots, L$. Without loss of generality, it is assumed that the norm of the spatial signature vector $\mathbf{a}_l^{[i]} = [a_{1,l}^{[i]}, \cdots, a_{N,l}^{[i]}]^T$ for each source's polarization is N, where $l = 1, \cdots, L$, $i = v, h$, and ^{T} denotes transpose. From (3), it is clear that $\mathbf{p}_l = [p_l^{[v]} \; p_l^{[h]}]^T$ has a unit norm. Thus, the strength of the source signals is absorbed in the magnitude of $s_l(t)$.

III. Comparison between different array configurations

We now compare an N-sensor dual-polarization linear array with two configurations of $2N$-sensor dual-polarized arrays, each is composed of single-polarized elements, as shown in Fig V. Each antenna of the dual-polarized array of dual-feed sensors has dual-feed points, as shown in Fig. 1(c). In the first dual-polarized array of single-polarized elements configuration (Configuration A in Fig. 1(a)), the array consists of N vertically polarized sensors followed by N horizontally polarized sensors, whereas in the second dual-polarized array of single-polarized elements configuration (Configuration B in Fig. 1(b)), the array consists of $2N$ sensors alternating between horizontal and vertical polarizations.

The combined data vector received at a dual-polarized antenna array is expressed in the following vector format

$$\mathbf{x}(t) = \begin{bmatrix} \mathbf{x}^{[v]}(t) \\ \mathbf{x}^{[h]}(t) \end{bmatrix} = \begin{bmatrix} \mathbf{A}^{[v]}\mathbf{P}^{[v]} \\ \mathbf{A}^{[h]}\mathbf{P}^{[h]} \end{bmatrix} \mathbf{s}(t) + \begin{bmatrix} \mathbf{n}^{[v]}(t) \\ \mathbf{n}^{[h]}(t) \end{bmatrix}. \tag{4}$$

The noise elements are modelled as stationary and white complex Gaussian processes with zero mean and variance σ^2 in each polarization, i.e.,

$$E\left[\mathbf{n}(t+\tau)\mathbf{n}^H(t)\right] = \sigma^2 \delta(\tau) \mathbf{I}_{2N}, \tag{5}$$

where $\delta(\tau)$ is the Kronecker delta and $\mathbf{I}_{2N}$ denotes the $2N \times 2N$ identity matrix.

In the underlying dual-polarized antenna arrays, we consider the closeness and distinctions of two sources using the correlation in both the spatial and polarimetric domains. It is clear from (4) that

$$\begin{aligned} \mathbf{a}_l &= \left[\left(p_l^{[v]}\mathbf{a}_l^{[v]}\right)^T \quad \left(p_l^{[h]}\mathbf{a}_l^{[h]}\right)^T \right]^T \\ &= [p_l^{[v]}a_{1,l}^{[v]}, \cdots, p_l^{[v]}a_{N,l}^{[v]}, \; p_l^{[h]}a_{1,l}^{[h]}, \cdots, \; p_l^{[h]}a_{N,l}^{[h]}]^T \end{aligned} \tag{6}$$

represents the joint spatio-polarimetric signature of the lth signal, $l = 1, \cdots, L$.

A. Dual-Polarized Array

We consider a structured mixing matrix for convenience. In this case, $\mathbf{a}_l^{[v]} = \mathbf{a}_l^{[h]} = \mathbf{a}_l$. Accordingly, the joint spatio-polarimetric signature of the lth signal for a dual-polarized array can be expressed as

$$\mathbf{a}_l^{(D)} = \mathbf{a}_l \otimes \mathbf{p}_l^{(D)}, \tag{7}$$

where $\otimes$ denotes the Kronecker product operator. In conventional single-polarized antenna arrays, a high spatial correlation may prohibit source resolution [7]. Therefore, reduction of the source spatial correlations becomes important which can be achieved by changing the array manifold. The new manifold is comprised of both source spatial and polarization signatures. The spatio-polarimetric correlation coefficient is defined as [8]

$$\begin{aligned} \beta_{l,m}^{(D)} &= \frac{1}{N}\left(\mathbf{a}_m^{(D)}\right)^H \mathbf{a}_l^{(D)} = \frac{1}{N}\left(\mathbf{a}_m \otimes \mathbf{p}_m^{(D)}\right)^H \left(\mathbf{a}_l \otimes \mathbf{p}_l^{(D)}\right) \\ &= \left(\frac{1}{N}\mathbf{a}_m^H \mathbf{a}_l\right)\left((\mathbf{p}_m^{(D)})^H \mathbf{p}_l^{(D)}\right) = \beta_{l,m}\rho_{l,m}^{(D)}, \end{aligned} \tag{8}$$

where ^{H} represents the Hermitian and $\rho_{l,m}^{(D)} = \left(\mathbf{p}_m^{(D)}\right)^H \mathbf{p}_l^{(D)}$ is the polarimetric correlation coefficient between sources l and m, and $\beta_{l,m} = (1/N)\mathbf{a}_m^H \mathbf{a}_l$ is the spatial correlation between these sources for an N-element linear array. The N-element array response vector, $\mathbf{a}_l$, is expressed as

$$\mathbf{a}_l = [1 \; e^{-j\theta_l} \; \cdots \; e^{-j(N-1)\theta_l}]^T, \tag{9}$$

where $\theta_l = 2\pi(d/\lambda)\sin\phi_l$, d is the interelement spacing of the array, λ is the wavelength and ϕ_l is the DOA of the lth source. The polarimetric correlation coefficient between two sources is given by

$$\rho_{l,m}^{(D)} = \cos\gamma_l \cos\gamma_m + \sin\gamma_l \sin\gamma_m = \cos(\gamma_l \mp \gamma_m). \tag{10}$$

B. Configuration A

When using a dual-polarized array composed of the augmentation of N vertically polarized sensors and N horizontally polarized sensors, the array response is

$$\mathbf{a}_l^{(A)} = \mathbf{a}_l \otimes \mathbf{p}_l^{(A)}, \tag{11}$$

with

$$\mathbf{p}_l^{(A)} = \left[\cos\gamma_l \quad \sin\gamma_l e^{-jN\theta_l}\right]^T. \tag{12}$$

Resembling (8), the spatio-polarimetric coefficient is

$$\beta_{l,m}^{(A)} = \beta_{l,m}\rho_{l,m}^{(A)}, \tag{13}$$

where $\rho_{l,m}^{(A)}$ is a function of the polarimetric correlation and DOAs and is expressed as

$$\begin{aligned}\rho_{l,m}^{(A)} &= \left(\mathbf{p}_m^{(A)}\right)^H \mathbf{p}_l^{(A)} \\ &= \cos\gamma_l\cos\gamma_m + \sin\gamma_l\sin\gamma_m e^{-jN(\theta_l-\theta_m)}.\end{aligned} \tag{14}$$

The spatio-polarimetric correlation is reduced for $\rho_{l,m}^{(A)} < 1$.

C. Configuration B

Similarly the spatial-polarimetric array response for configuration B is

$$\mathbf{a}_l^{(B)} = (\mathbf{a}_l \odot \mathbf{a}_l) \otimes \mathbf{p}_l^{(B)}, \tag{15}$$

where $\odot$ denotes the Hadamard product. The element-by-element product of the N-element array response, $\mathbf{a}_l$ results in the array response vector of a decimated array with twice the interelement spacing as the original, and

$$\mathbf{p}_l^{(B)} = \left[\cos\gamma_l \quad \sin\gamma_l e^{-j\theta_l}\right]^T. \tag{16}$$

Subsequently the spatio-polarimetric coefficient is

$$\beta_{l,m}^{(B)} = \beta_{l,m}^{(\uparrow)}\rho_{l,m}^{(B)}, \tag{17}$$

where $\beta_{l,m}^{(\uparrow)} = \frac{1}{N}\left(\mathbf{a}_m \odot \mathbf{a}_m\right)^H \left(\mathbf{a}_l \odot \mathbf{a}_l\right)$ is the spatial correlation for a N-element decimated array. The polarimetric correlation, which also contains a spatial component, is

$$\begin{aligned}\rho_{l,m}^{(B)} &= (\mathbf{p}_m^{(B)})^H \mathbf{p}_l^{(B)} \\ &= \cos\gamma_l\cos\gamma_m + \sin\gamma_l\sin\gamma_m e^{-j(\theta_l-\theta_m)}.\end{aligned} \tag{18}$$

It is evident from (17) that the array used in configuration B with half a wavelength interelement spacing generates a grating lobe problem when the spatial separation between

the two sources is high. To avoid the grating lobes, the array in configuration B must be spatially over-sampled such that $d \leq \frac{\lambda}{4}$. If the interelement spacing is reduced to $d = \frac{\lambda}{4}$, then the aperture of the array in configuration B becomes $\frac{2N-1}{4}$ which is roughly the same as $\frac{N-1}{2}$ for the dual-polarized array.

IV. Simulations

We compare the performance of three array configurations for polarimetric MUSIC-based DOA estimation. We also relate their performance to the sources' spatio-polarimetric correlation. Figure 2 compares the spatial correlation of an $N = 4$ element array with $d = \lambda/2$ and a decimated array with $d = \lambda$ for a source with a $\phi_1 = 10^\circ$. The effect of the spatial under-sampling is clearly demonstrated.

Figure 3 compares $\rho_{1,2}^{(D)}$, $\rho_{1,2}^{(A)}$ and $\rho_{1,2}^{(B)}$ for $\phi_1 = 10^\circ$ and $\gamma_1 = 45^\circ$. It can be seen that $\rho_{1,2}^{(D)}$ is independent of γ_2 meanwhile $\rho_{1,2}^{(A)}$ and $\rho_{1,2}^{(B)}$ vary with changes in γ_2. A grating area is shown in Figs. 3(b)-(d) due to the exponent in (14) and (18). Additionally, spatial over-sampling for the array in configuration B reduces the grating area in Fig. 3(d) as compared to Fig. 3(c). It is worth noting that the same spatial over-sampling eliminates the grating problem in the spatial correlation, $\beta_{1,2}^{(\uparrow)}$.

Figure 4 depicts the spatio-polarimetric correlations $\beta_{l,m}^{(D)}$, $\beta_{l,m}^{(A)}$ and $\beta_{l,m}^{(B)}$ versus the DOA and polarization angle parameters, ϕ_2 and γ_2. The dual polarized array does not exhibit a grating problem as can be seen in Fig. 4(a). The array in configuration A shows some grating area due to the exponent in (16), however, the grating area is lower than that in Fig. 3(b) due to the inclusion of the spatial correlation. The effect of spatial over-sampling is evident in the reduction of the grating area in Fig. 4(d), as compared to that of the decimated array exhibited in Fig. 4(c).

Figure 5 shows the performance comparison between the three arrays at hand for two different apertures. In Fig. 5(a), the apertures of all the arrays is kept equal to the aperture of the dual-polarized array. The performance of the dual-polarized array is comparable to that of the array in configuration B. In this case, the array in configuration B does exhibit the grating lobe problem, meanwhile the array in configuration A is spatially over sampled. In Fig. 5(b), the apertures of all the arrays is the same as the aperture of the array in configuration A. The performance of the dual-polarized array is also comparable to the

array in configuration B. On the other hand, the performance of the array in configuration A suffers from further loss of resolution compared to the other two arrays since its spatio-polarimetric correlation is not as low as its counterparts. It is worth noting that the dual-polarized array and the array of configuration B both suffer from the grating lobe problem in Fig. 5(b).

V. Conclusion

The paper compared the DOA performance of different configurations of multi-antenna receivers having single-polarized and dual-polarized double-feed antennas. All arrays have the same number of antennas with one half of the antennas of vertical polarizations and the other half of horizontal polarizations. The DOA performance of each array is viewed in terms of the respective polarimetric spatial correlation. To establish a common reference, the correlation is expressed in terms of a product of spatial correlation of a reference array and a modification that reflects the change in array configuration. The paper contrasted the reduction in correlation with the grating lobes that arise due to using the same array span.

References

[1] E. R. Ferrara and T. M. Parks, "Direction finding with an array of antennas having diverse polarizations," *IEEE Trans. Antennas Propagat.*, vol. 31, pp. 231–236, March 1983.

[2] J. Li and R. J. Compton, "Angle and polarization estimation using ESPRIT with a polarization sensitive array," *IEEE Trans. Antennas Propagat.*, vol. 39, pp. 1376–1383, Sept. 1991.

[3] Y. Zhang, M. G. Amin, and B. A. Obeidat, "The spatial polarimetric time-frequency distributions and their applicaiton to direction-of-arrival estimation," *Proc. SPIE*, vol. 5205, pp. 75–85, Aug. 2003.

[4] M. G. Amin and Y. Zhang, "Bilinear signal synthesis using polarization diversity," *IEEE Signal Processing Letters*, vol. 11, no. 3, pp. 338–240, March 2004.

[5] V. R Komanduri, A. Hoorfar, and N. Engheta, "Low-profile array design considerations for through-the-wall microwave imaging applications," *IEEE Inter. Symp. Antennas Propagat.*, Washington, DC, July 2005.

[6] Y. T. Lo and S. W. Lee, editors, *Antenna Handbook, Theory, Applications and Design*, Van Nostrand Reinhold, 1988.

[7] H.-C. Lin, "Spatial correlation in adaptive arrays," *IEEE Trans. Antennas Propagat.*, vol. AP-30, no. 2, pp. 212–222, March 1982.

[8] Y. Zhang and M. G. Amin, "Spatial and polarization correlations in array processing," *IEEE Sensor Array and Multichannel Signal Processing Workshop*, Barcelona, Spain, July 2004.

(a)Configuration A

(b)Configuration B

(c)Dual-polarized array

Fig. 1. Array configurations

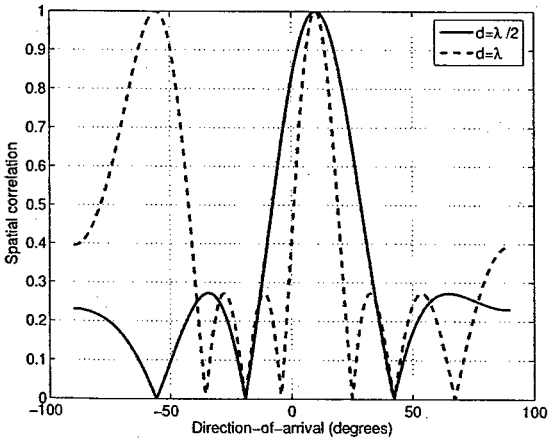

Fig. 2. Spatial correlation $\beta_{1,2}$ and $\beta_{1,2}^{(\dagger)}$

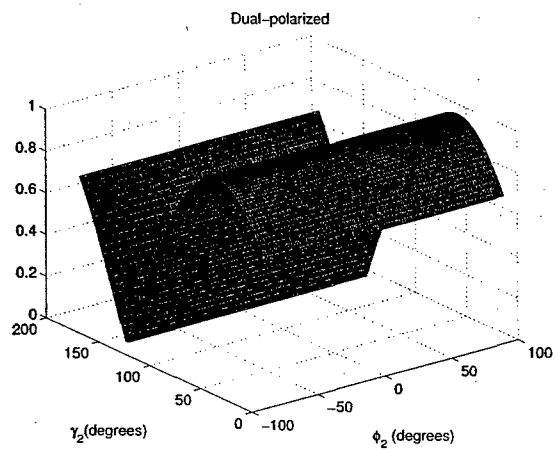

(a)$\rho_{1,2}^{(D)}$ independent of d

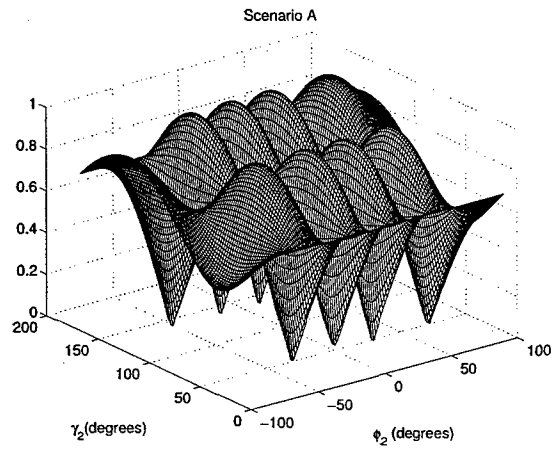

(b)$\rho_{1,2}^{(A)}$ for $d = \frac{\lambda}{2}$

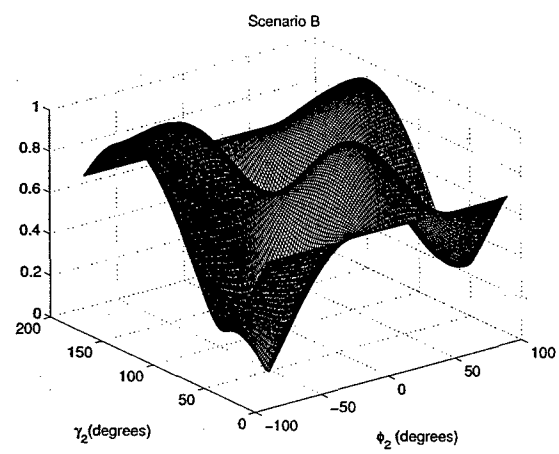

(c)$\rho_{1,2}^{(B)}$ for $d = \frac{\lambda}{2}$

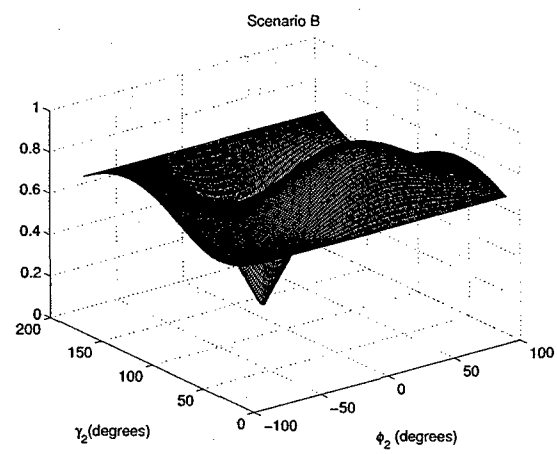

(d)$\rho_{1,2}^{(B)}$ for $d = \frac{\lambda}{4}$

Fig. 3. Comparison between $\rho_{l,m}^{(D)}$, $\rho_{l,m}^{(A)}$ and $\rho_{l,m}^{(B)}$

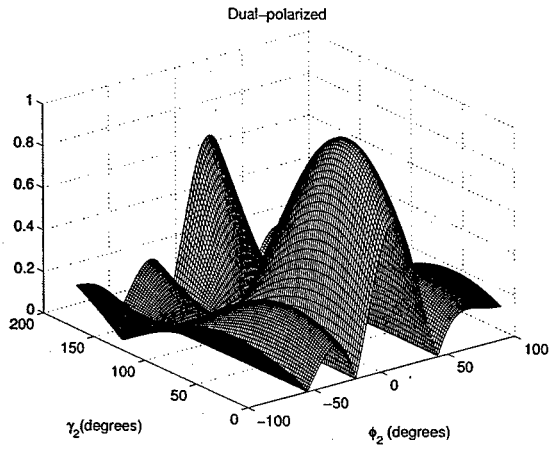

(a)$\beta_{1,2}^{(D)}$, independent of d

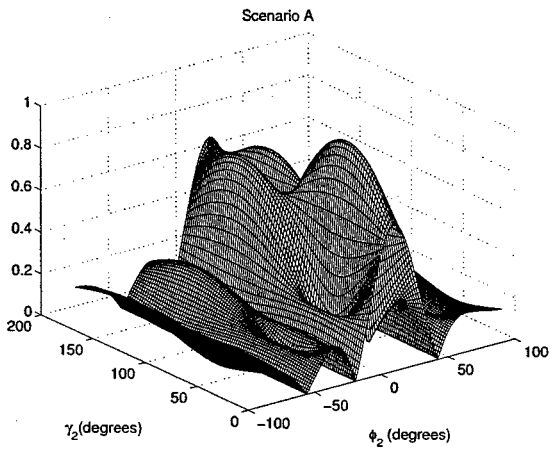

(b)$\beta_{1,2}^{(A)}$ for $d = \frac{\lambda}{2}$

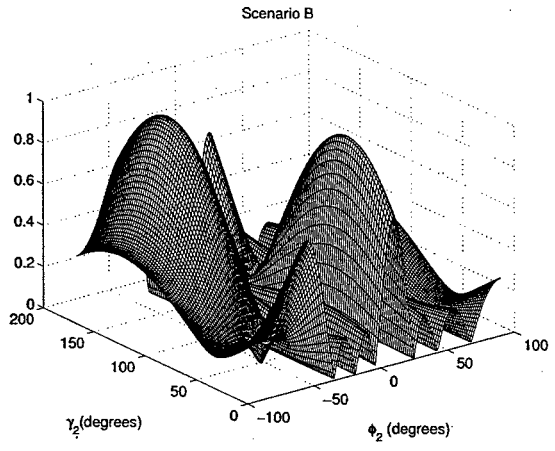

(c)$\beta_{1,2}^{(B)}$ for $d = \frac{\lambda}{2}$

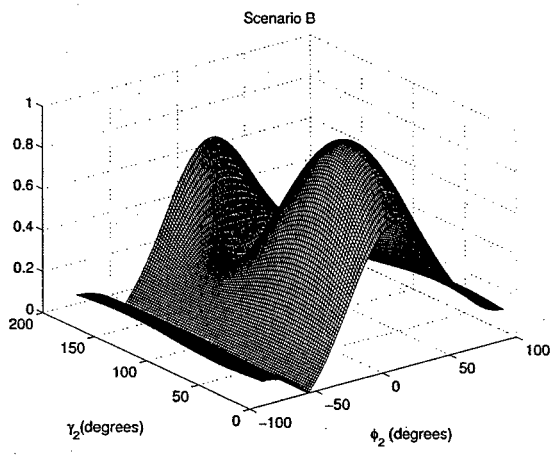

(d)$\beta_{1,2}^{(B)}$ for $d = \frac{\lambda}{4}$

Fig. 4. Comparison between $\beta_{l,m}^{(D)}$, $\beta_{l,m}^{(A)}$ and $\beta_{l,m}^{(B)}$

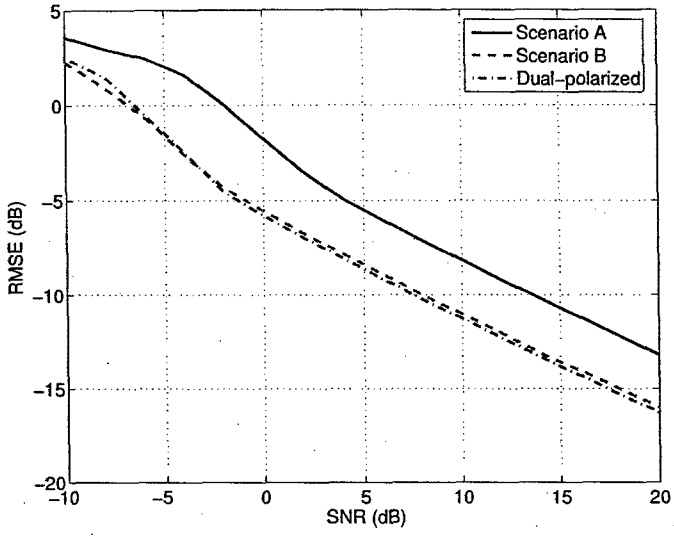

(a)Short aperture

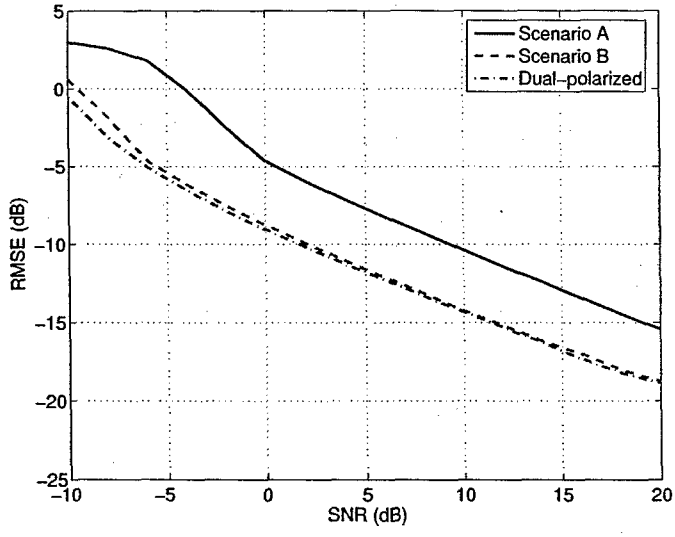

(b)Extended aperture

Fig. 5. Performance comparison for two different apertures

MICRO-DOPPLER EXPERIMENTS

Pawan Setlur, Moeness Amin, and Fauzia Ahmad

Abstract

Targets in real life have vibrating and rotating parts in addition to the translations endured by the target. The target itself might either be rotating or vibrating with no translation, a motion is described mechanically as simple-harmonic motion (SHM). Such nonlinear motions then induce additional frequency modulations around the Doppler, this is termed micro-Doppler effect. Micro-Doppler has many applications for target recognition and classification. We have conducted several indoor experiments in the Radar Imaging Lab at the Center for Advanced Communications at Villanova University, for detecting micro-Doppler. Experiments were designed to image targets which induce micro-Doppler like signatures. The targets were primarily a rotating fan and a toy train moving on a circular track. The experiments were conducted using CW (Continuous Wave) radars. These radars measure only the real component of target returns. Time-frequency techniques were used to depict the instantaneous frequency of the target. The objective of the experiments was to compute the frequency of vibrations or rotations. In the ensuing sections, we introduce the problem statement, and propose a model for Micro-Doppler. Experimental setup is described, and simulation and experimental results are also presented.

I. INTRODUCTION

The effect of nonuniform, rotational or non-linear motion on target signatures and characteristics was extensively studied in the past [1]. However, only recently, returns from rotational/vibrational motions of targets, termed micro-Doppler, have been investigated [2, 3]. The term "micro" is primarily used for two main reasons i) Smaller sidebands about the Doppler. ii) Micro motions of targets, compared to large displacements involved in translations [4]. Micro-Doppler captures certain dynamics of the target, which aid in target classification and recognition [3, 4, 5], as every target has distinctive micro motion dynamics. Fourier based methods have inherent resolution problems. Hence, high resolution time-frequency methods are employed [3, 4].

Vibrational/rotational target endure SHM. Hence, irrespective of the model chosen, whether a rotation model or a vibrational model, the target signature will be sinusoidal in the time frequency plane. Moreover, the Doppler frequency also exhibits SHM, with the same resonant frequency as the target.

II. MODEL

A micro-Doppler signal can be parameterized by,

$$x(t) = \exp(j2\pi \cos(\omega_v t - \phi)) \tag{1}$$

where ω_v is the frequency of vibration/rotation.

The instantaneous frequency $IF(t)$ can be written as,

$$IF(t) = -\omega_v \sin(\omega_v t - \phi) \tag{2}$$

which satisfies

$$\frac{d^2}{dt^2}(IF(t)) + \omega_v^2 IF(t) = 0 \tag{3}$$

Equation (3) is the differential equation for undamped SHM (Simple Harmonic Motion). Hence, the instantaneous frequency $IF(t)$ exhibits SHM with the same resonant frequency. It must be noted that rotation is also SHM. This can be proven when we consider the motion to be projected onto the diameter of the circular trajectory of the target. Therefore, in practicality, we do not need another rotation model to describe targets having turning motions. Figure 1 is the 3D schematic of a radar and a target enduring SHM. If the target has an instantaneous range given by

$$\mathbf{r}(t) = \mathbf{d}\cos(\omega_v t) \tag{4}$$

$$\mathbf{d} = d[\cos(\alpha_t)\cos(\beta_t), \cos(\alpha_t)\sin(\beta_t), \sin(\alpha_t)]^T \tag{5}$$

Then, the instantaneous frequency of such a setup can be written as

$$f_i(t) = -2 f_c / c \; \omega_v d \sin(\omega_v t)(\mathbf{n}_\mathbf{r})^T \mathbf{n}_\mathbf{t} \tag{6}$$

$$\mathbf{n}_\mathbf{r} = (\cos(\alpha_r)\cos(\beta_r), \cos(\alpha_r)\sin(\beta_r), \sin(\alpha_r))^T \tag{7}$$

$$\mathbf{n}_\mathbf{t} = (\cos(\alpha_t)\cos(\beta_t), \cos(\alpha_t)\sin(\beta_t), \sin(\alpha_t))^T \tag{8}$$

Here, ω_v is the resonant or fundamental frequency of the SHM of the target, $\mathbf{d}$ is the maximum displacement of the target from the origin, and f_c is the carrier frequency of the radar. The pairs (α_t, β_t) and (α_r, β_r) are the elevation and azimuth of the target and radar respectively. Clearly, equation (6) gives rise to a sinusoidal signature in the time-frequency plane.

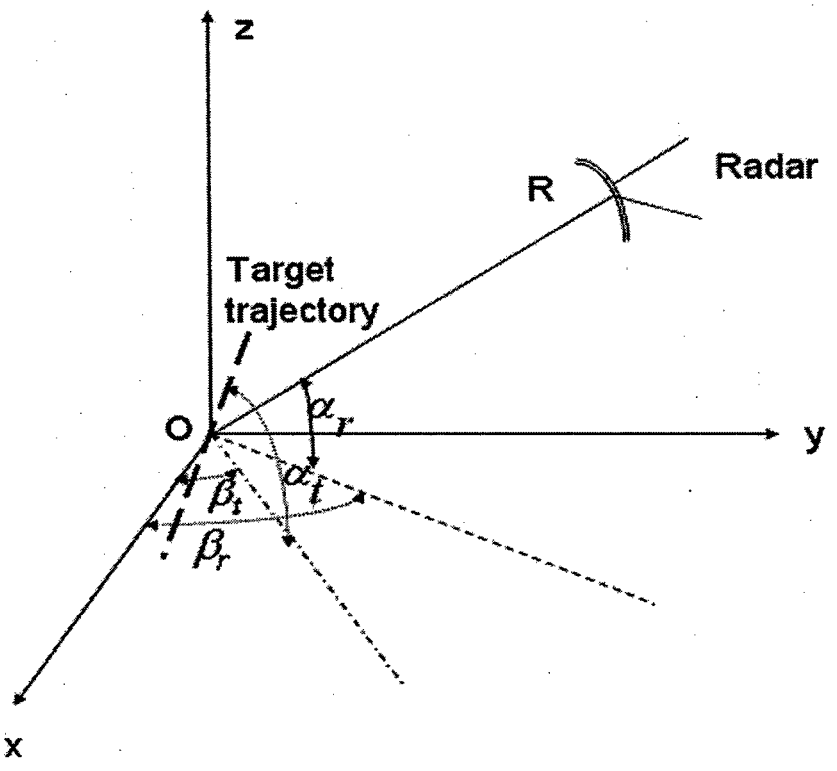

Figure 1. Geometry of the scene

III. HARDWARE SETUP

The 24 GHz and 10 GHz CW (Continuous wave) radars were used for imaging targets undergoing micro-Doppler like motion. The radar units used measure only the real components of the baseband returns. Hence, additional signal processing must be performed to properly analyze the returns. An A/D converter was used to digitize the analog returns. The A/D converter can operate on 8 different single channels simultaneously. An application, written in Visual Basic® on Microsoft .Net® platform, is used to set the sampling rate and communicate with the A/D converter. Figure 2 depicts the collection of main hardware and radars. Figure 3 depicts a snapshot of the application used to interface the A/D with a laptop.

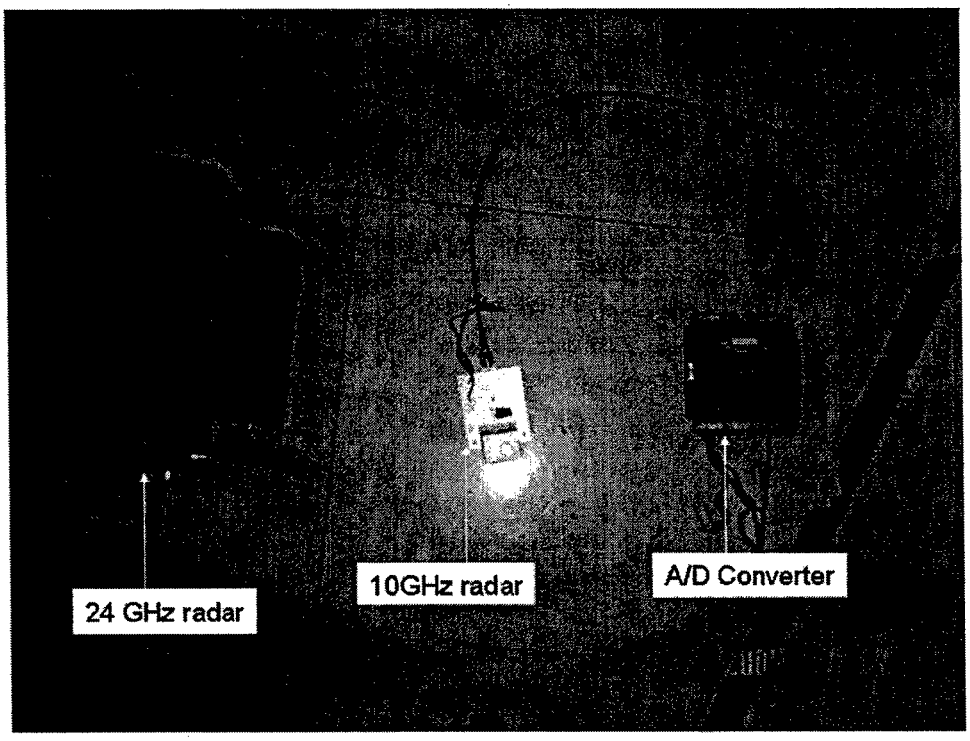

Figure 2. Hardware used, Left to right: 24 GHz, 10 GHz Radars and an A/D converter

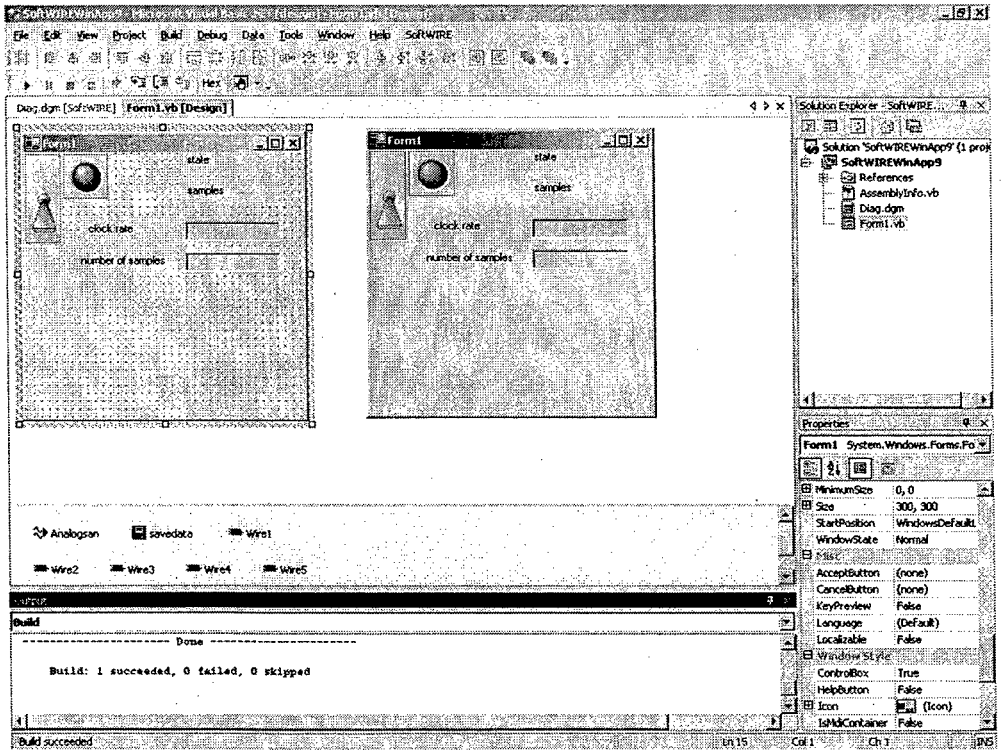

Figure 3. Snapshot of application.

We chose CW radars as they are affordable, robust to clutter, and perform exceptionally well in highly cluttered environments frequently encountered in indoor imaging.

IV. DATA COLLECTION

We have performed three experiments producing various types of micro-Doppler signatures. These are: high micro-Doppler for rotating fans, very low micro-Doppler for a toy train moving on a circular track, and low frequency components for a corner reflector moving back and forth at a slow rate. We will describe the experimental setup in the ensuing sub-sections. However, we digress to bring other important aspects to light. If $x(t)$ is the real signal, and $H\{\cdot\}$ denotes the Hilbert transform operation, the analytic signal $y(t)$ is then given by

$$y(t) = x(t) + jH\{x(t)\} \tag{9}$$

The baseband micro-Doppler signal has no carrier and has an instantaneous frequency on both sides of 0 Hz. Hence, the transformation in (9) will mirror the negative instantaneous frequency onto the positive side. This can be seen in Figure 4, which shows the pseudo Wigner-Ville distribution of the analytic signal, after performing transformation (9) on a simulated real micro-Doppler signal. Figure 5 is the pseudo Wigner-Ville distribution of the complex signal. Note that Figure 5 is the actual target signature.

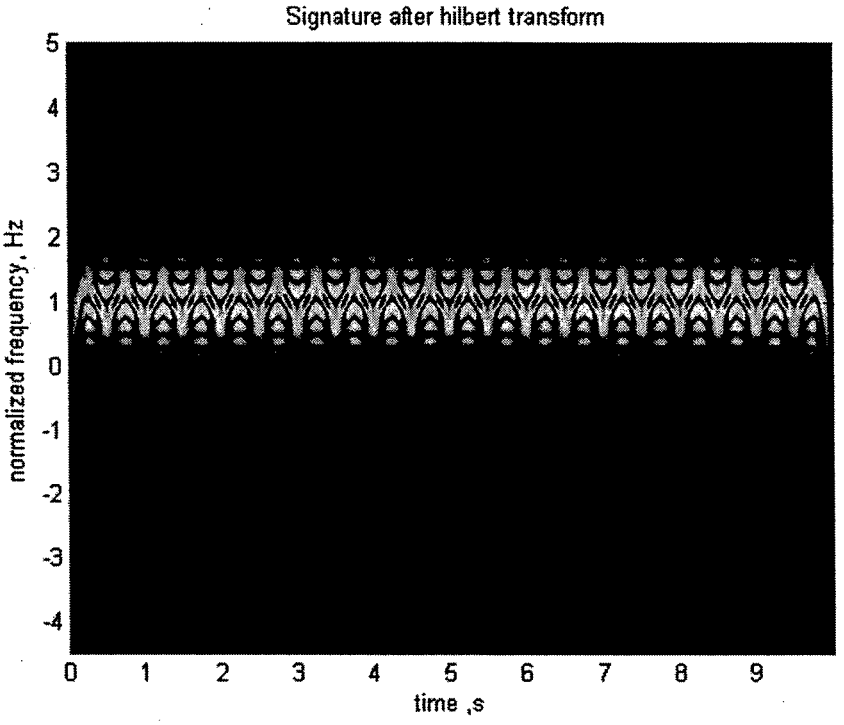

Figure 4. Analytic signal's signature.

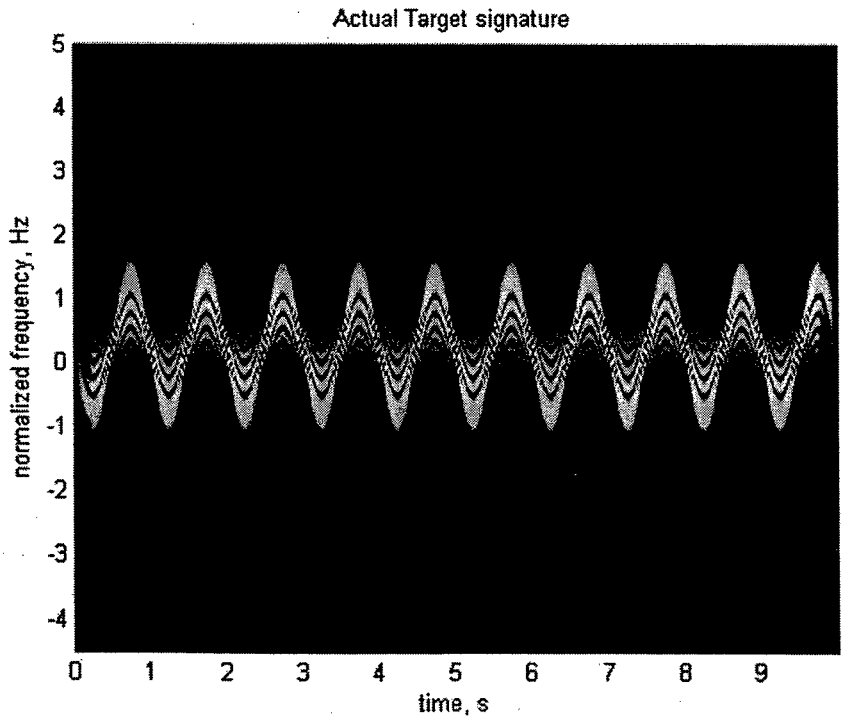

Figure 5. Complex signal's signature (Actual Target signature).

The inherent drawback of using real signals, therefore, is that the frequency components are symmetric (replicated) on either side of the frequency axis. In our case, since the signal frequency spectrum is centered at 0Hz, we expect to see replicas around 0Hz. For micro-Doppler detection, this replica can be misinterpreted as another target. For example, in Figure 6, we compute the pseudo Wigner-Ville for a real micro-Doppler signal with $\omega_v = 2\pi$ Hz and $\phi = 0$ in (1). The Figure indicates two targets having vibrations 180° out of phase with each other. In reality, however, there is only one target. Since we have apriori information about the experiments, radar output, and target positions, we can ignore the replica and consider only the target signature.

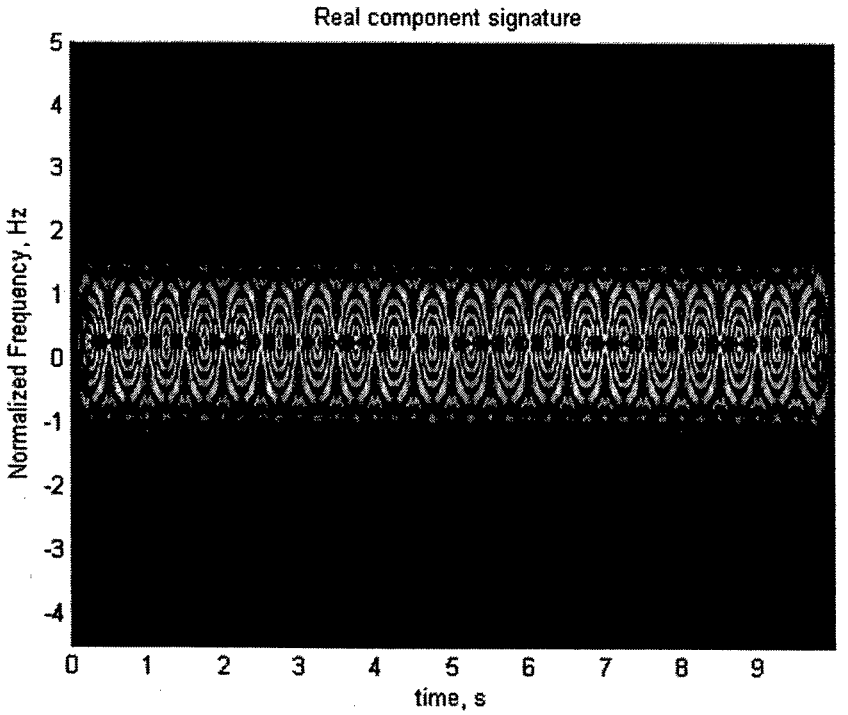

Figure 6. Real signal's signature.

V. EXPERIMENTAL SETUP

We have conducted three different experiments, showing the micro-Doppler signatures of objects that could be found in indoor radar imaging, namely (a) Corner reflector moving back and forth over an arms length, (b) Rotating fan, (c) Toy train.

V.1. Corner Reflector

The corner reflector echoes most of the transmitted energy back to the radar. The corner reflector, used in the experiment and shown in Figure 7, was held by a person and moved back and forth slowly in front of the radar. The initial distance from the radar is 5 ft. The sampling frequency used is 100Hz for a duration of 5 seconds. The 10 GHz radar was used to image the target.

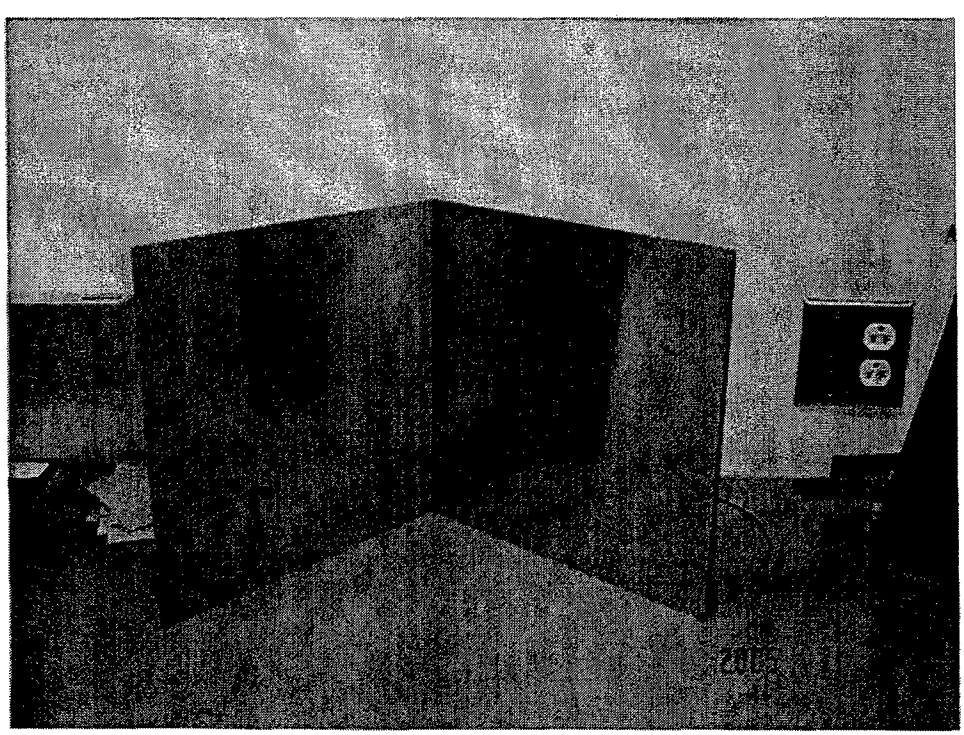

Figure 7. Corner reflector used in experiment A.

V.2. Rotating fan

The fan is portable and has a height of approximately 3 feet from the ground. It has 3 plastic blades. We covered one blade with aluminum foil so that the returns from the other two blades are not seen by the radar. The fan and the experimental setup are shown in Figure 8. High frequency micro-Doppler components are expected from a rotating fan. The sampling frequency must be high enough, so that the window used in the time- frequency distribution can capture the non-stationarity of the signal. We simulated a rotating fan using $\omega_v = 10\text{Hz}$ and $\phi = 0$ in equation (1). We set the sampling frequency to 100Hz and 1000Hz, and computed the pseudo Wigner-Ville distribution for both cases. In Figure 9, the fan's returns are sampled at 100Hz and the signal length is 1000 samples. In Figure 10, the sampling frequency is 1000Hz and number of samples are 1000. The window size for the pseudo Wigner-Ville is the same in both cases. Figure 9 does not depict the signal's instantaneous characteristics, but rather the overall spectrum of the harmonics. On the other hand, Figure 10 clearly shows the instantaneous frequency.

The sampling frequency used in the fan experiment was thereby set to 1000Hz for a duration of 1 second. The base of the fan is at a distance of 4 feet from the radar. The 24 GHz radar was used in the experiment.

V.3. Toy train on a circular track

The toy train in the experimental setup can be seen in Fig. 11. The diameter of the circular track is 15.5 inches. The body of the train is made of plastic. The returns we expect are low frequency micro-Doppler signals. The sampling frequency used in this experiment is 100Hz for a duration of 17 seconds. Aluminum foil was draped onto the body of the train, except the wheels. The 10 GHz radar was used for this experiment.

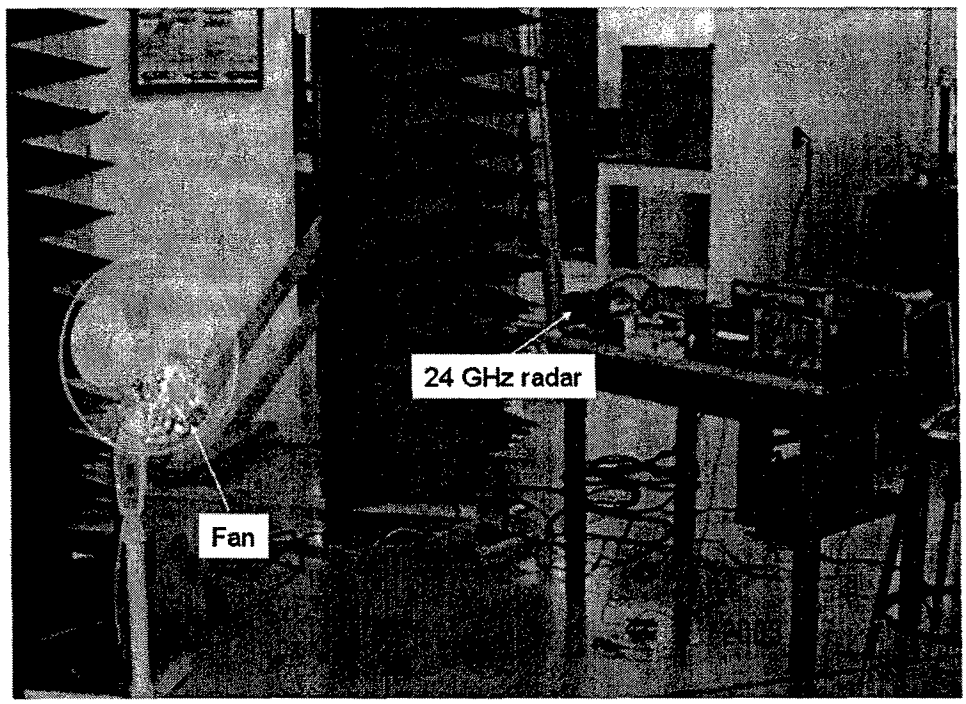

Figure 8. Layout of the fan experiment. The 24 GHz radar can be seen at the left end of the table.

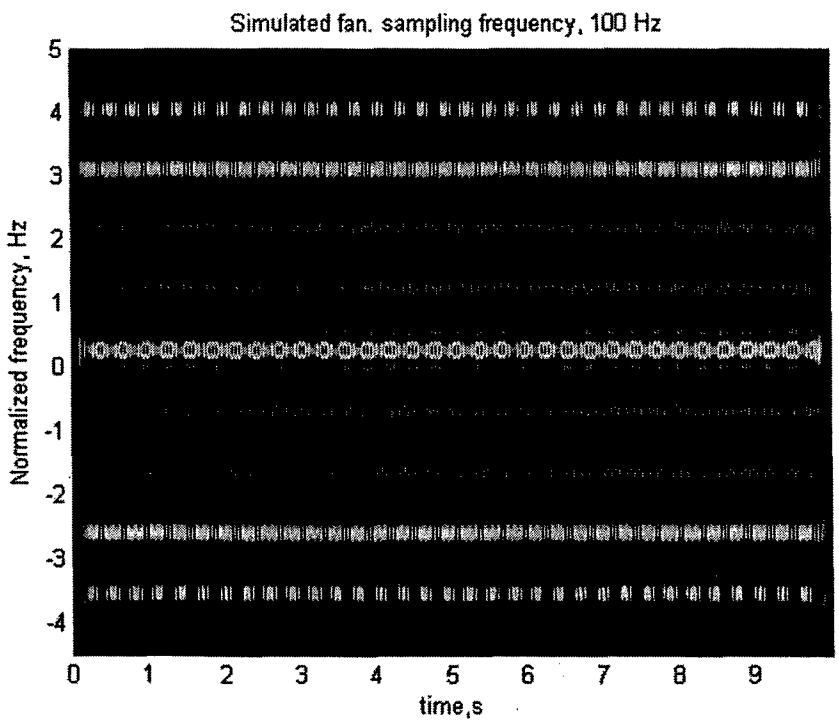

Figure 9. Simulated fan-sampling frequency of 100 Hz

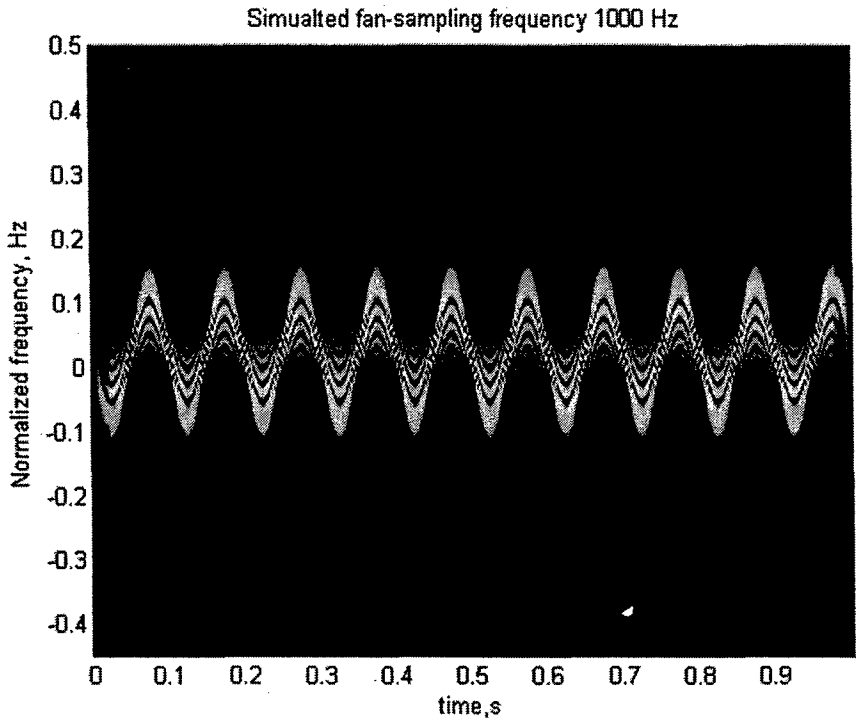

Figure 10. Simulated fan-sampling frequency of 1000 Hz

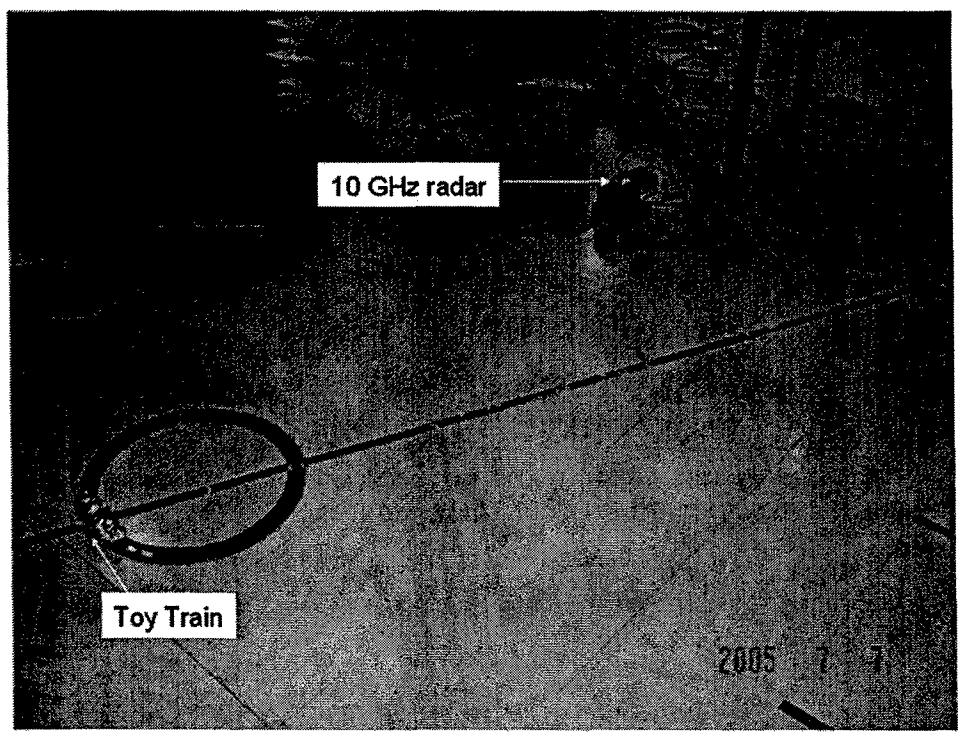

Figure 11. Layout of the toy train experiment. The 10 GHz radar can be seen on top of the 24 GHz radar.

VI. RESULTS

In all experiments, we used the pseudo Wigner-Ville distribution to illustrate the instantaneous frequency. Figure 12 depicts the sinusoidal signature for Experiment (A). Due to the replicas and the aliasing effects in the time frequency plane, the time period cannot be definitively estimated. The results of Experiment (B) are shown in Fig. 13, where we can observe two signatures. This is due to using the real signal, as previously discussed. However, since we are interested in only estimating the resonant frequency, we can ignore one of the signatures. The rotation rate of the fan is estimated to be approximately 750rpm. An interesting observation, from 0.6-1 second in Figure 13, is that the time period of rotations decreases. This occurred because the aluminum foil on the blade unexpectedly slackened and hindered the smooth operation of the fan.

Figure 14 illustrates the results of Experiment (C). As observed from the figure, the toy train has a time period of about 7.5 seconds for a single rotation. A stop watch was also used to measure the time period. The experimental values were in close agreement with the measured values. At time instants 3.5 and 11 seconds, pulse like events (more specifically, narrow sinc like functions) are seen in Fig. 14. The difference in time for the events is equal to the time period of one full rotation. The train has a metallic rod connecting the rear wheels, one end of which is highly reflective. The pulse like events are caused by the highly reflective end of the rod, which is exposed to the radar over a short period within one rotation.

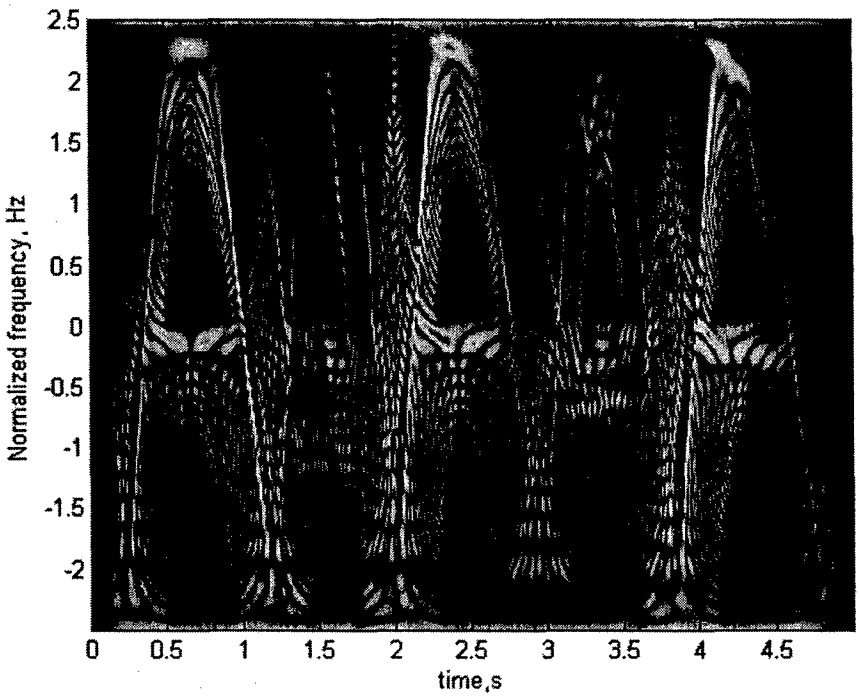

Figure 12. Results of experiment A

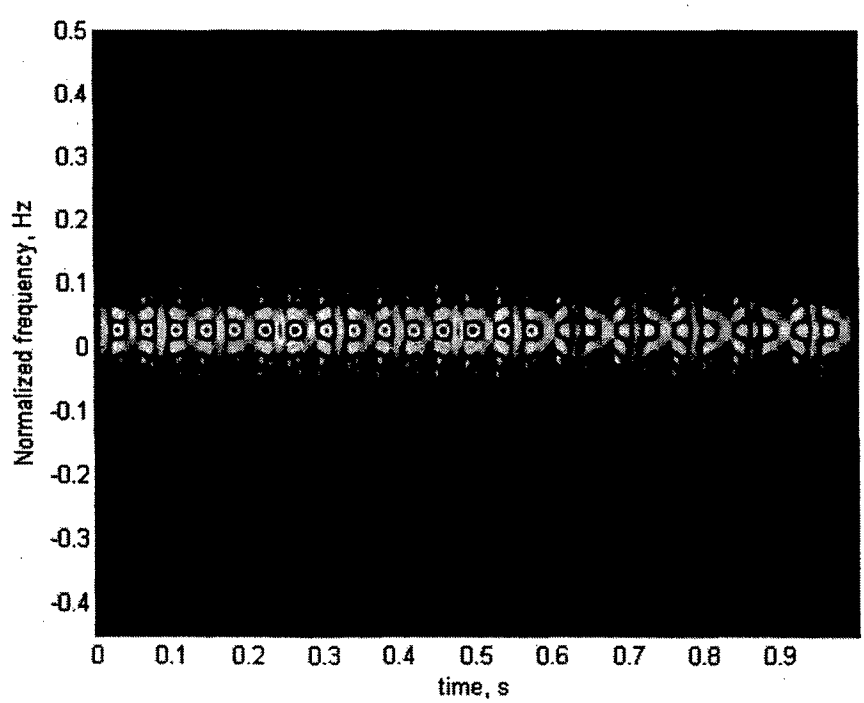

Figure 13. Results of experiment B

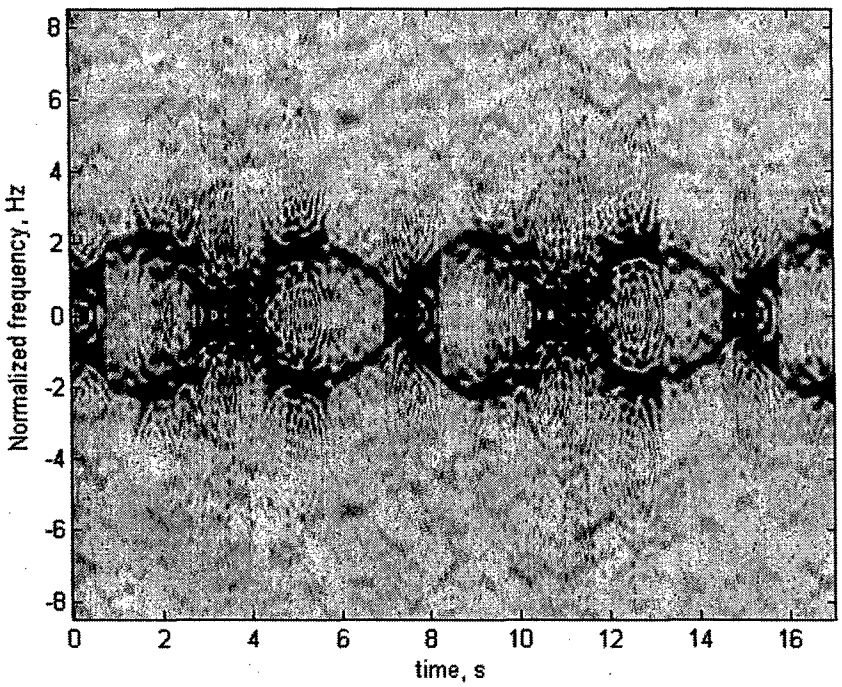

Figure 14. Results of experiment C

VII. REFERENCES

[1] J. E. Gray, "The Doppler spectrum for accelerating objects". Proceedings of the IEEE International Radar Conference, pp: 385-390, Arlington, VA, USA, May 1990.

[2] V. C. Chen and H. Ling, *Time frequency transforms for radar imaging and Signal analyses*, Artech house, 2002.

[3] V. C. Chen, F. Li, S. -S. Ho and H. Wechsler, "Analysis of micro-Doppler signatures". IEEE Proceedings Radar, Sonar and Navigation, Volume: 150, Issue: 4, pp: 271-276, 1 August 2003.

[4] T. Thayaparan, S. Abrol, V. C. Chen and E. Riseborough, "Analysis of micro-Doppler radar signatures from experimental helicopter and human data". NATO SET-080 symposium, Oslo, Norway, 11-13 October 2004.

[5] R. Kleinman, R. Mack, "Scattering by linearly vibrating objects," IEEE Transactions on Antennas and Propagation, 27 May 1979.

ONR FY05 Collection Data

REPORTING PERIOD: 1 October 2004 to 30 September 2005

NAME OF PI: Moeness AMIN

UNIVERSITY/Contractor: Villanova University

TITLE OF PROJECT: Classification and Discrimination of Sources with Time-Varying Frequency and Spatial Spectra

GRANT/CONTRACT/WORK REQUEST NUMBER: N00014-98-1-0176

1. Papers published in referred journals (TITLE; JOURNAL):

Y. Zhang, B. Obeidat, and M. G. Amin, "Spatial polarimetric time-frequency distributions for direction-of-arrival estimations," IEEE Transactions on Signal Processing (in press).

Y. Zhang, K. Yang, and M. G. Amin, "Subband array implementations for space-time adaptive processing," EURASIP Journal on Applied Signal Processing, vol. 2005, no. 1, pp. 99-111, Jan. 2005.

2. Books or Book chapters published (TITLE; AUTHORS/EDITORS; PUBLISHER):

Y. Zhang, B. Obeidat, and M. G. Amin, "Polorimetric time-frequency MUSIC for direction finding of moving sources with time-varying polarizations," in S.Chandran (ed.), Advances in Direction of Arrival Estimation, Boston, MA: Artech House (in press).

3. Patents (ANNOTATE EACH WITH FILED OR GRANTED):

None

4. Presentations (INVITED):

"Signal Processing and Beamforming Techniques in Wideband Through-the-Wall Radar Imaging," Keynote Speaker, SPIE Defense & Security Symposium, Conference on Digital Wireless Communications VII, Orlando, FL, March 2005.

5. Presentations (CONTRIBUTED):

Y. Zhang, B. Obeidat, and M. G. Amin, "Nonstationary array processing for sources with time-varying polarizations," Annual Asilomar Conference on Signals, Systems, and Computers, Pacific Grove, CA, Nov. 2004.

B. Obeidat, Y. Zhang, and M. G. Amin, "DOA and polarization estimation for wideband sources," Annual Asilomar Conference on Signals, Systems, and Computers, Pacific Grove, CA, Nov. 2004.

B. A. Obeidat, Y. Zhang, and M. G. Amin, "Nonstationary array processing for tracking moving targets with time-varying polarizations," IEEE International Conference on Acoustics, Speech, and Signal Processing, Philadelphia, PA, March 2005.

B. Obeidat, M. G. Amin, Y. Zhang, A. Hoorfar, "Sensor configuration in polarized antenna arrays," IEEE International Symposium on Signal Processing and its Applications, Sydney, Australia, Aug. 2005.

P. Setlur, M. Amin, and T. Thayaparan, "Micro-Doppler signal estimation for vibrating and rotating targets," IEEE Internal Symposium on Signal Processing and its Applications, Sydney, Australia, August 2005.

B. A. Obeidat, Y. Zhang, and M. G. Amin, "Performance analysis of DOA estimation using dual-polarized antenna arrays," IEEE International Symposium on Signal Processing and Information Technology, Athens, Greece, Dec. 2005.

P. Setlur, M. Amin, F. Ahmad, and T. Thayaparan, "Indoor imaging of targets enduring simple harmonic motion using Doppler radars," IEEE International Symposium on Signal processing and Information Technology, Athens, Greece, Dec. 2005.

6. Honors (Presidential YIP, elections to Fellow status in major scientific society; appointed editor of scientific journal, elected NAS/NAE/IOM, awarded medal by scientific society, Chairman of scientific meeting, etc):

Served on the Franklin Institute Committee on Science and the Arts (on-going)

7. Number of graduate students:

One-graduate student (full-time)

8. Number of Post-doctoral students:

One half-time Postdoctoral Fellow

9. Number of undergraduate students supported:

None

10. Number of under-represented members by group:

None

REPORT DOCUMENTATION PAGE

Form Approved
OMB No. 0704-0188

1. REPORT DATE *(DD-MM-YYYY)*	2. REPORT TYPE	3. DATES COVERED *(From - To)*
10/03/2005	Interim	October 2004 - November 2005

4. TITLE AND SUBTITLE

Classification and Discrimination of Sources with Time-Varying Frequency and Spatial Spectra

5a. CONTRACT NUMBER

5b. GRANT NUMBER

N00014-98-1-0176

5c. PROGRAM ELEMENT NUMBER

6. AUTHOR(S)

Amin, Moeness, G. (PI)

5d. PROJECT NUMBER

5e. TASK NUMBER

5f. WORK UNIT NUMBER

7. PERFORMING ORGANIZATION NAME(S) AND ADDRESS(ES)

Villanova University
800 Lancaster Ave
Villanova, PA 19085

8. PERFORMING ORGANIZATION REPORT NUMBER

Acct: 527616

9. SPONSORING/MONITORING AGENCY NAME(S) AND ADDRESS(ES)

Office of Naval Research
Ballston Centre Tower One
800 North Quincy Street
Arlington, VA 22217-5660

10. SPONSOR/MONITOR'S ACRONYM(S)

11. SPONSOR/MONITOR'S REPORT NUMBER(S)

12. DISTRIBUTION/AVAILABILITY STATEMENT

Approved for Public Release; Distribution is Unlimited.

13. SUPPLEMENTARY NOTES

14. ABSTRACT

The research objective in FY05 evolved around the moving target tracking using time-frequency signal representations. In addition to achieving these objectives, the research has progressed on three other fronts, namely, Sensor configuration in polarized antenna arrays, direction-of-arrival (DOA) and polarization estimation for wideband sources, and Micro-Doppler experiments. We have developed polarimetric time-frequency MUSIC (PTF-MUSIC) for effective localization of targets with distinct polarization signatures, and confirmed the applicability and effectiveness to tracking of moving targets with time-varying polarization signatures. We have evaluated the DOA estimation performance of different receiver configurations employing double-feed dual-polarized array as well as arrays of single-feed single-polarized elements. We have also conducted several indoor experiments and investigated the micro-Doppler characteristics of targets with vibrating and rotating parts.

15. SUBJECT TERMS

Time-frequency distribution, direction-of-arrival (DOA) estimation, polarization, wideband, micro-Doppler

16. SECURITY CLASSIFICATION OF:			17. LIMITATION OF ABSTRACT	18. NUMBER OF PAGES	19a. NAME OF RESPONSIBLE PERSON
a. REPORT	b. ABSTRACT	c. THIS PAGE			19b. TELEPHONE NUMBER *(Include area code)*
U	U	U	UU	73	